Arabian Journal of Geosciences

Detecting of new alteration zones for gold exploration at the Barramiya District, Central Eastern Desert of Egypt using ASTER data and geological field verification

--Manuscript Draft--

Manuscript Number:	AJGS-D-12-00632
Full Title:	Detecting of new alteration zones for gold exploration at the Barramiya District, Central Eastern Desert of Egypt using ASTER data and geological field verification
Article Type:	Original Paper
Abstract:	Abstract In the present study, the use of ASTER data and fieldwork supported by mineralogical and geochemical investigations enabled detecting of new alteration zones promise targets for gold exploration in the particular ultramafic-mafic successions at the Barramiya district. Processing of Advanced Spaceborne Thermal Emission and Reflection Radiometer (ASTER) band ratios (4/8, 4/2, 8/9) successes in recognizing of two alteration zones (area 1 and area 2) of listwaenite alterations in the north east and south east of the Barramiya gold mine. The Barramiya district is made up of ophiolitic ultramafic belts of serpentinites, talc carbonates and talc graphite schists, mainly thrusted over the metavolcanic sequences. They include highly strained and tectonized parts enriched in sulphides, iron oxides and carbonates, with developed listwaenite alterations along the thrust contacts. Gabbro and granitic intrusions were intruded in the ultramafics and metavolcanic rocks. The structural setting of the Barramiya district has an important role for the distribution of gold mineralization since the alteration zones are concordant with the main NE-SW structural trend. Mineralogical studies and X ray diffraction (XRD) analysis revealed that area1 and area2 are of propylitic alteration consisting of talc, ankerite, magnesite, quartz and calcite. Ore microscope studies revealed the sulphides as main ore mineral assemblages carrying gold within these alteration zones, moreover, goethite crystals and malachite are present as accessory minerals. The Fire assay method for gold in the Barramiya mine shows Au content in the range of 5.04 ppm in the graphite schist, 4.02 ppm in the quartz veins and 3.76 ppm in the listwaenite alterations. The result of atomic absorption analysis of samples from area 1 reveals an average Au content in the quartz-veins of 2.4 ppm, Ag content is 8.0 ppm and Cu content is 2.4 wt%. The listwaenite alterations show an average Au content of 4.4 ppm and a Cu content of 2.8 wt%. In area 2, the atomic absorption analysis of the quartz-veins revealed an average Au content of 2.6 ppm, an Ag content of 6.2 ppm and a Cu content of 1.9 wt%. The listwaenite alterations of area 2 include 3.5 ppm of Au and 2.4 wt% of Cu.

Detecting of new alteration zones for gold exploration at the Barramiya District, Central Eastern Desert of Egypt using ASTER data and geological field verification

S. M. Salem [1], N. M. Soliman [1], T. M. Ramadan [1] and R. Ö. Greiling [2]

[1]National Authority for Remote Sensing and Space Sciences(NARSS), Cairo, Egypt.

[2]Karlsruhe Institute of Technology, Institut für Geowissenschaften, Hertzstrasse 16, D-76187, Karlsruhe, FR Germany

Abstract

In the present study, the use of ASTER data and fieldwork supported by mineralogical and geochemical investigations enabled detecting of new alteration zones promise targets for gold exploration in the particular ultramafic-mafic successions at the Barramiya district. Processing of Advanced Spaceborne Thermal Emission and Reflection Radiometer (ASTER) band ratios (4/8, 4/2, 8/9) successes in recognizing of two alteration zones (area 1 and area 2) of listwaenite alterations in the north east and south east of the Barramiya gold mine. The Barramiya district is made up of ophiolitic ultramafic belts of serpentinites, talc carbonates and talc graphite schists, mainly thrusted over the metavolcanic sequences. They include highly strained and tectonized parts enriched in sulphides, iron oxides and carbonates, with developed listwaenite alterations along the thrust contacts. Gabbro and granitic intrusions were intruded in the ultramafics and metavolcanic rocks. The structural setting of the Barramiya district has an important role for the distribution of gold mineralization since the alteration zones are concordant with the main NE-SW structural trend. Mineralogical studies and X ray diffraction (XRD) analysis revealed that area1 and area2 are of propylitic alteration consisting of talc, ankerite, magnesite, quartz and calcite. Ore microscope studies revealed the sulphides as main ore mineral assemblages carrying gold within these alteration zones, moreover, goethite crystals and malachite are present as accessory minerals. The Fire assay method for gold in the Barramiya mine shows Au content in the range of 5.04 ppm in the graphite schist, 4.02 ppm in the quartz veins and 3.76 ppm in the listwaenite alterations. The result of atomic absorption analysis of samples from area 1 reveals an average Au content in the quartz-veins of 2.4 ppm, Ag content is 8.0 ppm and Cu content is 2.4 wt%. The listwaenite alterations show an average Au content of 4.4 ppm and a Cu content of 2.8 wt%. In area 2, the atomic absorption analysis of the quartz-veins revealed an average Au content of 2.6 ppm, an Ag content of 6.2 ppm and a Cu content of 1.9 wt%. The listwaenite alterations of area 2 include 3.5 ppm of Au and 2.4 wt% of Cu.

Keywords: Ultramafics; Ophiolitic rocks; ASTER images; Lithological discrimination; Alteration zones; Gold mineralization.

I. Introduction

The Neoproterozoic evolution of the Arabian-Nubian Shield (ANS) in NE Africa is traditionally regarded as a result of accretion of intra-oceanic island arcs, fragments of oceanic lithosphere (ophiolites), oceanic plateaus, and continental micro-plates during the consolidation of Gondwana (Gass, 1982; Stern, 1994; Kröner et al., 1994; Abdelsalam and Stern, 1996; Johnson and Woldehaimanot, 2003). Increasing attention has been paid to features associated with the late-orogenic extension of the orogen because of its importance in ore deposits formation (Burke and Sengör, 1986; Wallbrecher et al., 1993; Greiling et al., 1994; Blasband et al., 2000).

The regional distribution pattern of mineral deposits in the Arabian-Nubian Shield (ANS) was mapped and described at different scales by a number of authors (Garson and Shalaby, 1976; Al Shanti et al., 1978; Sillitoe, 1979; Pohl, 1979, 1984 and 1988; Delfour, 1980; Jackson, 1986; Agar 1992). Collisional tectonics involve geologic processes producing high amounts of fluids that may subsequently contribute to the formation of ore deposits when expelled from deeper parts of an orogen (Oliver, 1986; Nesbitt, 1992; Garven et al.,1999). Gold occurrences in the ANS are mainly confined to quartz-mineralized shear zones, VMS and epithermal deposits (Mahd adh Dhahab for example), which occur in the ophiolitic sequences, island arc assemblages in the late-orogenic Hammamat and Dokhan groups and in post-orogenic granitoids. Geochemical investigations of different rocks in the ANS (e.g. serpentinites, basalts, clastic sedimentary rocks) indicate gold concentrations of 20 to 50 ppb in mafic rocks and clastic sediments, and concentrations close to 200 ppb in serpentinites (Langwieder, 1994). Post-orogenic intrusions predating the quartz veins or shear zones provided heat sources for hydrothermal convection cells and interstitial waters dissolved available mineral species. Where convection cells were present, low concentrations of gold were derived from the host rocks due to elevated temperature and pressure. The hydrothermal fluids precipitated their dissolved mineral content as silica and quartz (Langwieder, 1994). Harraz, 1999 described the alteration zones as active mineralogical-chemical reaction areas formed in the country rocks due to the effect of the upcoming hydrothermal solutions, through metasomatism of CO_2, H_2O, K and subordinately Na as determined by mass balance calculations on the whole rock. Gold-rich deposits can be formed at all stages of the evolution of an orogen, in such a way that different types of gold deposits may be juxtaposed or overprinted on each other in host-rock sequences in arcs, back-arcs or accretionary prisms (Groves et al., 2003). The most common types of deposit include gold-rich syngenetic massive sulphide deposits, (Zierenberg et al., 1993; Hannington et al., 1998) or shear zone-hosted orogenic types of gold deposits (Groves et al., 1998; Goldfarb et al., 2001), although in some belts, auriferous porphyry copper deposits may also be important (Kesler et al., 2002). Johnson et al (2011) studied the of the history of the Arabian–Nubian Shield in concern with the depositional, plutonic, structural, and tectonic events with the closing stages of the northern East African Orogen. He mentioned that, the sutures, typically reactivated as transpressional/transcurrent zones, are located across the shield.

Gold production in Egypt seems to have started as early as the pre-dynastic times, about 4000 B.C., as several localities with gold mineralization exploited in these times are known in the Eastern Desert of Egypt (Hume, 1937; Kochin and Bassiuni 1968). The ancient Egyptians have exploited gold-bearing quartz veins from open pits and underground mines in spite of their primitive technology. During the middle of 20th century, particularly between 1932 and 1958, some of the major gold occurrences including Barramiya were examined and put under exploitation (El-Ramly et al., 1970). Botros (2004) offered a three-fold classification of gold deposits in Egypt, these are: strata-bound deposits, non strata-bound deposits, and placer deposits. The strata-bound deposits are subdivided into three-main types: gold-bearing algoma-type banded iron formation, gold-bearing tuffaceous sediments, and gold-bearing volcanogenic massive sulphide deposits. Non strata-bound deposits are divided into two main types: vein-type mineralization hosted in a wide range of rocks, and disseminated-type mineralization hosted in hydrothermally altered rocks (alteration zones). Placer deposits are divided into modern placers and lithified placers.

The Barramiya gold mine is a known landmark in the Central Eastern Desert of Egypt, located in the western part of the Barramiya district. It stopped its production since 1964. The Barramiya district had been subjected to several geological investigations for the exploitation of gold. These investigations include those of Ibrahim (1942), El-Alfy (1946), Attia (1948), El-Zoghby (1953), Amin (1955), Sabet and Zaatout (1955), Mansour et al., (1956), El-Shazly (1957,1959). El Shafei et al. (1983) used the heap-leach method for gold analysis in the quartz veins and gave gold contents of 2.5, 4.75 and 9.23 g/t. Botros (2004) recorded gold concentrations at the Barramiya mine of 2.74 g/t in graphite schist, 1.59 g/t in quartz veins and 1.37 g/t in listwaenites. In the Barramiya mine, gold mineralization within carbonaceous, listwaenized serpentinite and adjacent to post-tectonic granite stocks points toward a significant role of listwaenitization in the ore genesis. The tectonized serpentinite is altered to listwaenite through talc-actinolite schist and talc carbonate rock as the intensity of carbonatization increases near steeply dipping transpressive faults (Zoheir and Lihman 2011). Listwaenite is exposed as a several hundred meters long,

~ 100 m-wide elongate body at the mine area along an ~ E–W-trending dextral fault and adjacent to a sheet-like granitoid body. Ali-Bik et al (2012) studied the characteristics, petrogenesis and evolution of Barramiya Serpentinite and revealed the talc-magnesite deposits in the altered zones and their potentiality as targets for gold exploration.

Earlier, the gold was mined from stocks of quartz veins, plugs and dykes in the different rock types in restricted localities. Most of these localities were exploited by ancient Egyptians. Recently, the hydrothermally altered rocks have received considerable attention for gold exploration in the Eastern Desert because of their huge tonnages within relevant rock types and of their potential economic implications and favorable spectral characteristics for remote identification (Abrams et al.,1977 and 1983; Goetz et al., 1983; Podwysocki et al., 1983; Kruse et al., 1993; Crosta et al., 2003; Rowan et al., 2003 and Galvao et al., 2005).

Remote sensing techniques have progressed to advanced levels that are useful for lithological mapping as well as for identifying mineral deposits (Abrams et al., 1983; Sultan et al., 1986; Kaufmann 1988; Abrams and Hook, 1995; Mars and Rowan, 2006 and Gad and Kusky, 2006). These investigators used composite bands ratio images together with supervised classification techniques for lithological mapping of serpentinite rocks in the Barramiya area. Spectral absorption variations associated with altered rocks caused by hydrothermal activity can be detected on satellite images that are used as a rapid and inexpensive technique for determining the mineralogy and chemical composition of the alteration zones. The variables characterizing absorption features can be directly related to the mineralogy of the sample (Van Der Meer, 1999). The launch of ASTER in December 1999 provided higher spectral resolution data than ETM+ that enabled mineral exploration, particularly for areas with poor background information (Di Tommaso and Rubinstein, 2007). ASTER has three sensors to measure and record the reflected and emitted Electromagnetic Radiation (EMR). They are working in different wavelength regions the Visible and Near Infrared (VNIR) between 0.52 and 0.86 lm, Short Wave Infrared (SWIR) between 1.6 and 2.43 lm, and Thermal Infrared (TIR) between 8.125 and 11.65 lm (Table1). ASTER data consists of 14 spectral bands 3 VNIR, 6 SWIR, and 5 TIR with 15, 30, and 90 m spatial resolution, respectively. The VNIR, SWIR and TIR wavelength regions provide complementary data for lithological mapping. The ASTER multispectral imagery has offered improved spectral and spatial detail referring to ETM+ and has been shown to be effective in identifying alteration zones and mapping clastic and carbonate in different geologic environments moreover, predicting the occurrence of certain mineral groups and specific minerals (kaolinite, alunite, illite, muscovite, montmorillonite, chlorite, calcite, dolomite, serpentine, and others. Azizi et al. (2007) used ASTER-SWIR in the detection of hydrothermal alterations in east Zanjan, northern Iran, also Gabr et al (2010) used ASTER data to detect gold potential alteration zones in the acidic volcanics of Abu Marawat area (~100km north of the Barramiya mine).

The aim of the present study is the exploration of new gold occurrences in the listwaenites alterations in the ultramafic rocks of the Barramiya district. For this purpose, ASTER data has been used in detecting sites for gold exploration, verified by field geology involving mineralogical and geochemical analyses.

2. Geological setting

The studied area lies in the Central Eastern Desert of Egypt in the midway between Marsa Alam and Idfu, along an asphaltic road connecting the two towns. It is located between latitudes 25° 00' to 25° 12' North and longitudes 33° 46' to 34° 02' East, covering a surface of about 700 km^2 of moderate topography (Fig.1).

The Barramiya district was previously studied by Hume (1907, 1934) and Attia (1948), who described the serpentinites and their related rocks as intrusions of ultrabasic-basic rocks, namely dunites and peridotites rich in iron magnesium and calcium silicate minerals, mainly olivine and pyroxene. Mansour et al. (1956) described the geology of the Umm Salatit-El Hisinat belt in the Barramiya district as a series of schistose metasediments, ultrabasic-basic rocks and granites. The ultrabasic rocks are of peridotite origin, hydrothermally altered and composed of antigorite-serpentinite, associated with talc-carbonate rocks. The Egyptian Geological Survey and Mining Authority (EGSMA) maps of Wadi Barramiya area (1992 and 2000) show that the serpentinite and talc-carbonate rocks of the Barramiya district occur as slices up to several kilometers long, located along major ductile and brittle ductile shear zones. Hussein (1990) mentioned that gold deposits at Barramiya mine were divided by miners who exploited them into four lodes, referred to as: Main Lode; Tylors Lode; Caunter Lode and New Caunter Lode. The basement complex of the Barramiya district comprises Neoproterozoic ophiolitic mélange of allochthonous blocks and clasts of serpentinite and carbonatized/silicified derivatives tectonically incorporated in variably deformed metasedimentary and volcani-sedimentary rocks (Zoheir and Lihman 2011).

3. Methodology

3. 1. Remote sensing data

The remote sensing analyses supported by geological field studies, mineralogical and geochemical investigations performed in the present investigation, are the main tools used for detecting gold-bearing listwaenite alteration zones in the Barramiya district. ASTER data (Level 1B image gathered in May 2006), covering the Barramiya district and its surroundings, have been used to establish a more detailed surface geology and a better determination of the alteration zones. The ASTER data were geometrically and radiometrically corrected and UTM georeferenced. The images were then enhanced to improve the appearance of the image features before undertaking band combinations in red, green and blue (RGB). Spectral analyses of the alteration minerals in the detected alteration zones were obtained by matching the unknown spectra of their pixels to the U.S. Geological Survey (USGS) mineral library. A number of band combinations was manipulated and processed by using ERDAS Imagine 9.2, ENVI 4.7 and Arc GIS software on a Sunspark workstation at the Digital Analysis Laboratory of NARSS. The VNIR and SWIR data processing was normalized and converted to relative reflectance using the Flat Field method (Roberts et al., 1986). The digital numerical (DN) data were converted to relative reflectance using the assumption that the recorded DN is linearly related to the surface reflectance (Yamaguchi and Naito, 2003). We also consider that the image does not suffer atmospheric influences because the study area is located in a dry, sparsely vegetated area. The input radiance parameters of the ASTER instrument constrain the radiance values to a reflectance of 70% to avoid signal saturation over bright targets (ASTER User's guide, 2001). The ASTER 30-m resolution SWIR data were re-sampled to correspond to the VNIR 15-m spatial dimensions. Nearest neighbor re-sampling method uses the nearest pixel values without any interpolation so it was used to maintain the original pixel values of the image. The 15-m resolution 6 SWIR and 3 VNIR bands were combined to form 9-band 15 m spatial resolution data sets. Several approaches and techniques such as image classification (unsupervised classification), False-color composite (FCC), principal component analysis, (PCA) Constrained Energy Minimization (CEM), Spectral Feature Fitting (SFF) and band ratios were used in distinguishing the country rock types, the structural elements and the alteration zones for gold exploration.

3.1.1. Unsupervised classification

This tool uses naturally occurring statistical groupings in the spectral data to determine the clusters into which the data will be classified into similar spectral signature. In an unsupervised classification, we do not know what features are actually at any specified location, but we want to aggregate each of the locations into one of a specified number of groups or clusters. Each cluster is statistically separate from the other clusters based on the values for each band of each cell within the clusters. The statistics establishing the cluster definition are stored in a signature file.

3.1.2. ASTER false colour composite (FCC)

The false color composite image bands (7, 3, 1) in R, G, B is a helpful method for clarifying the lithological discrimination, regional lineaments and structural pattern of the study area.

3.1.3. ASTER Principal Component Analysis (PCA)

Principal Component Analysis (PCA) is used to produce uncorrelated output bands, to segregate noise components, and to reduce the dimensionality of data sets. This is done by finding a new set of orthogonal axes that have their origin at the data mean and that are rotated so that the data variance is maximized. Nine bands PCA are constructed from the original 9-band (VNIR & SWIR) ASTER image. From the output PCA 9-bands we selected three bands (PC3, PC4, and PC2) for better illustration of the structural elements affecting the study area.

3.1.4. Constrained Energy Minimization (CEM)

It is a technique used to map the distribution of some mineral assemblages and the abundance of significant minerals. The strengths of the CEM technique are its ability to deal with a variety of spectral backgrounds and to accommodate nonlinear mixing among background materials (Farrand and Harsanyi, 1997). Also, the Spectral Feature Fitting (SFF) is a mapping method available in ENVI software that compares the fit of (CEM) image spectra to reference spectra using a least-squares technique.

3.1.5. Band combination and band ratio transformation analysis

A series of ratio images and matched filter processing have been used for analyzing the VNIR+SWIR spectral reflectance data (Green et al., 1988; Ruse et al., 1993; Harsanyi and Change, 1994; Boardman et al., 1995; Rowan & Mars, 2003), as well as spectral-angle mapper processing (Kruse et al., 1993; Gillespie et al., 1998). These authors used extensively these methods as computationally rapid means of displaying compositional information while subduing reflectance related to albedo and topographic slope variations (Rowan et al., 1974; among others). The SWIR wavelength region relative band-depth (RBD) images of RBD6: (band 4+band 7)/ (band 6*2) and RBD8: (band 7+band 9)/ (band 8*2) are useful for displaying the intensities of Al-OH, Fe, Mg-OH and CO_3 absorption (Crowley et al., 1989; Rowan & Mars, 2003).

In this study, different image processing and ratios have been experimented, the band ratios (4/8, 4/2, 8/9) of ASTER image proved to be the best for better discrimination between hydrothermally altered and unaltered rocks in the study area. The alteration minerals are characterized by an absorption factor close to 2.165 μm for the group of Al-OH-bearing minerals such as pyrophyllite and alunite. Jarosite represents sulfide minerals and has an absorption factor of 2.260 µm. Minerals with an absorption factor close to 2.327 µm belong either to CaCO3- or Mg-OH-bearing minerals, a group which includes calcites, chlorites, and talc. The group of minerals which has an absorption factor close to 2.205 µm is represented by montmorillonite, kaolinite, muscovite, and illite. Although it is not be possible to map the distribution of particular minerals using ASTER imagery, it is possible to differentiate between the above mentioned mineral groups.

3. 2. Geological Field verification and sampling

Based on remotely-sensed data and interpretation, an intensive geological field work was done by the authors to check out the results given by the remote sensing data. During the geological field verification, one hundred and thirty representative samples from the rock varieties of the target zones in the Barramiya district have been collected for analytical techniques. These representative samples were selected depending upon their apparent mineral composition especially those enriched in altered and opaque ore minerals.

3. 3. Analytical techniques

Mineralogical study and X ray diffraction (XRD) analysis have been carried out at the Department of Mineralogical Investigation of the Egyptian Mineral Resources Authority (EMRA) to determine the mineralogical composition of the different rock types and to identify the altered minerals and the types of carbonates in the detected alteration zones. Reflection ore microscope studies, Scanning Electron Microscope (SEM) (type EHM=1000, Mag=1.20KX, Signal A=SE2, Leo 1530, WD=5.7mm.) and Electron Dispersion X ray Analysis (EDXA) were performed on 35 polished specimens from the target zones at the Institutes of Geology and Physics of Karlsruhe University, Germany. This has been done to determine the mineral assemblages associated with gold occurences. Geochemical analyses were carried out to the same samples at EMRA laboratories as follows: 15 samples were chosen from the graphite schists, quartz veins and listwaenites (5 samples from each) for fire assay analysis to assess the gold content in the Barramiya mine. A total of 20 samples from both of the alteration zones area 1 and area 2 (10 samples from each) representing the quartz veins and listwaenites were selected for atomic absorption analysis (Model GBC-908) to detect the gold, silver and copper in these target zones. Moreover, 10 samples more from each of area 1 and area 2 were subjected to fire assay analysis to confirm the presence of the gold in the quartz veins and listwaenite alterations which were detected by atomic absorption analysis in these areas.

4. Results

4.1. Interpretation of the processed ASTER data

4.1.1. Unsupervised classification

The unsupervised classification method of Aster image yielded a compiled geological map at scale1:100,000 based on the geological maps of Wadi El Barramiyaarea of EGSMA (1992, 2000) and (Zoheir and Lihman 2011). The compiled map shows good overview and pattern, as well as lineaments, general structure features in NE-SW and ENE-WSW trends and lithological discrimination for the study area. The geological field work revealed homogeneity (to some extent) of the unsupervised classification compiled map with Zoheir and Lihman map 2011(Figs 2a.&2b). However, the calcareous metagrawack metasiltstone quartz-chlorite sericite schist of Zoheir map was incorporated with the bassltic andesite in the compiled map (grouped as one unit) because they are so mixed and interference and have fairly similar spectral signature. Moreover, the compiled map failed to separate the post tectonic granite and the Nubian sandstone (grouped them as a same spectral reflectance) due to quartz enrichments in both units. However, we converted the compiled map into vector map and could distinguish the Nubian sandstone (pale yellow colour) (in the western side of the map) from the post tectonic granite (Fig.2c).

4.1.2 False-color composite (FCC)

Applying of Aster (FCC) color composite image of bands (7, 3, 1) provided an excellent base map reflecting the main geological and lineament features. Lithological discrimination has been recognized in the FCC, the ultramafic rocks appear in dark green color, the basic metavolcanics in dark brown, the acidic metavolcanics in pale brown, the gabbro-diorite suite in brown, the tonalite in yellowish brown and the Nubian sandstone in the southwestern corner of the mapped area appear in pale greenish brown color (Fig.3a).

4.1.3. Principal Component Analysis (PCA)

The selected PC3, PC4, and PC2 enabled to delineate the main geologic structures such as faults, shear zones and fractures that affect on the Barramiya district in the NE-SW and ENE-WSW trends and control the gold mineralization in this area (Fig.3b).

4.1.4. Constrained Energy Minimization (CEM)

The application of CEM image enables to map the locations of serpentinite rocks and their distribution in the study area, displaying them in deep brownish red color on ASTER image (Fig.3c). The comparable SFF of the serpentinites have, also, been clearly shown in (Fig.3d).

4.1.5. Band ratio images

Using the RBD of RBD6: (band 4+ band 7)/ (band 6*2) and RBD8 (band7+ band9)/ (band 8*2) helped in recognizing the intensities and distribution of altered Mg-OH and CO3 minerals The ultramafic rocks appear in light purple color in ASTER image (Fig.3e). Moreover, the Band ratios (4/8, 4/2, 8/9) of the ASTER image enable the detection of two intense alteration zones (area1 and area2) that appear in deep yellowish red color (Figs.3f&3g) respectively.

4.2. Field description

4.2.1 Geology of Barramiya district

The Barramiya district is built up of discontinuous ophiolitic ultramafic belts comprising serpentinite, talc-carbonate, talc graphite and ferrugenated quartz-carbonate listwaenite ridges. They form NE-SW trending parallel sheets, fragments and blocks thrusted over the island arc metavolcanic rocks at Gabal Barramiya and Gabal Umm Salatit (Fig. 4a). One of the prominent features in the ultramafics is the presence of linear zones of serpentinites showing extreme alterations along thrusts and shear zones with development of gold-mineralized listwaenite ridges (Fig. 4b). Listwaenite is composed of Fe–Mg carbonate, quartz and Cr-bearing with disseminated chromite and accessory pyrite and arsenopyrite. An intense carbonatization is closely related with gold mineralizations consisting of a characteristic paragenesis arsenopyrite, pyrite, chalcopyrite, pyrrhotite, sphalerite, galena and sulfosalts (e.g. Kerrich and Fyfe, 1981; Phillips and Brown, 1987).The metavolcanics are of basaltic andesite and dacitic rhyolite composition associated with volcanoclatics and tuffs. Another significant feature of magmatic highlands is the existence of large plutonic intrusions of tonalite and gabbro diorite penetrating into the ultramafics and metavolcanic rocks (Fig. 4c). Post tectonic monzogranites as a later stage of granitic intrusion associated by quartz veins and veinlets were intruded and offshooted in the tonalite and gabbrodiorite complex. In the west of the study area, the ultramafics and metavolcanic rocks are unconformably overlain by Cretaceous Nubia Sandstone. All kinds of metamorphic basement rocks, ophiolites (ancient oceanic lithosphere) and magmatic arcs can be observed in the Barramiya district. So the district seems to display a particular potentiality for including gold resources within its different alteration zones and structural domains. Thus the Barramiya is an area with high gold potential in Egypt.

4.2.2. Structural setting of Barramiya district

The basement rocks of the Barramiya district form domains of high strain zones of a complex network phases of deformations. An early phase was represented by folding (with plunge angle

50-60° in the NE), foliation in the ENE-WSW trend (with dip angle 40-50° in SW) and thrusting and shear zones (with lenses range from 50 to 100m, wides 3-5m, trending NE-SW with dip angles 60^0-75^0in the SE) developed in the old ophiolite members and adjacent metavolcanics. This was followed by second phase of tight isoclinal and recumbent folds related with less abundant NW-SE ductile shear zones affected in the ophiolite rocks. Finally the third phase of deformation was expressed by crenulation and mineral lineation, rods, boudinage structure and kink bands (with angle plunge 10-30^0 in the SE) that coeval with happening of dextral transpression (along the major thrust planes) and formation of mega shear zones in the ultramafics and metavolcanics. In the high strain zones, the rocks are typically foliated in the NE-SW trend with dip angle 60^0 with developed pervasive cleavages and locally pencil fabrics formed by the intersection of two or more closely-spaced fracture sets, as well as spaced fractures and joints. At different places the ultramafics are thrusted over the metavolcanics. Within the main shear zones and tension fractures in the central part of the study area, a well developed mineral lineation and mylonitic fabrics can be observed (Fig.4 d). The linear fabric is assumed to represent the direction of relative tectonic transport of units of metavolcanic and serpentinite rocks, the kinematic indicators suggest dextral sense of movement. The orientation of the mineral lineation, fold axes, pencils, rods and other minor structures in the area show constant trends of NNE-SSW, ENE-WSW and NE- SW. The structural setting of the study area is a tool for tracing alteration zones since they occur along the NE-SW and ENE-WSW trending faults and shear zones and fractures.

4.2.3. Geology and structure of the Barramiya gold mine

Within the Barramiya area, Barramiya gold mine is located at the intersection of latitude 25° 04' 24'' N and longitude 33° 47' 16'' E. It is situated in the eastern limb of a synclinal fold, succeeded by an anticlinal fold in the eastern part of the mine area, the axes of these folds trend mainly NE–SW. The Barramiya gold mine is built of dismembered blocks and slices of serpentinite incorporated and intermixed in an intensively deformed matrix of tremolite-actinolite and graphite schist (Fig. 5a). The mineralized zone at this mine is hosted in graphite schist stocked by quartz veins and altered listwaenite ridges. The main gold-quartz lode is associated with some quartz veinlets that traverse the main body of rocks along the fold axes. The fabric trends E–W and is parallel to the main gold-quartz lode.

4.2.4. Geology and structure of the alteration zone area 1

This alteration zone lies 7 km northeast of Barramiya mine covering a surface area of about $7km^2$.

The altered rocks were developed along fault planes, folding, shear zones and around thrust contacts of the ultramafics on the basaltic andesite rocks of this area. It is hosted in the ultramafic rocks, characterized by intense alteration consisting of serpentinites, talc carbonates, listwaenite ridges and quartz veins and veinlets, pervasive through these altered rocks. These veins range in thickness from 10 cm to 1 m, and in lengths up to hundereds of meters, extending in the ENE-WSW trend. This alteration zone is massive, yellowish brown to kaky color, contains sulphides, goethite crystals and green stainings of malachite (Fig.5b). The type of alteration is propylitic in which the minerals with an absorption factor of about 2.327 μm belong either to CaCO3- or Mg-OH-bearing minerals, a group including calcite, chlorite and talc.

4.2.5. Geology and structure of the alteration zone area 2

This alteration zone lies 4 km southeast of Barramiya mine covering a surface area of about 10km^2 extended in the E-W trend. The altered rocks of this area were developed along fault planes, folding, shear zones and around thrust contacts of the ultramafics on the dacitic rhyolite rocks. As in the alteration zone in area 1, this alteration is hosted in the ultramafic rocks, consisting of serpentinites, talc carbonates, talc graphite, listwaenite ridges and quartz veins (extend in the NE-Sw and ENE-WSW trend with thicknesses up to 1m. and lengths up to 1km.), veinlets and offshoots cut through these rocks (Fig.5c). It is massive, yellowish brown to kaky in color. A lot of sulphide, iron oxide crystals and green malachite patches are scattered on the surface of this alteration zone. Calcite, ankerite and talc minerals form the alteration minerals in this zone.

4.3. Mineralogy and geochemistry

4.3.1. Mineralogy

The results of mineralogical examination will be described as follows;

4.3.1. 1. Petrography

The petrographical study of the different rock units in the Barramiya district revealed that the serpentinites rocks are made up of antigorite and chrysotile as main mineral constituents. Talc, calcite and ankerite are present as altered minerals filling fractures (Fig.6a). Opaque minerals of chromite, sulphides and iron oxides are accessory minerals. The listwaenites are composed of quartz and carbonates with accessory opaque minerals. Many quartz crystals show undulose extinction and serrate contacts which refer to deformation and shearing. A lot of fractures were observed in most quartz and carbonates of the listwaenites. This is an evidence of compression. These fractures were considered as paths for mineralized fluids (eg Harraz, H.Z., 1999 and

Taylor and El Kazzaz, 2002); hence they appear filled with ore minerals (Fig.6b). The talc graphite schist is composed mainly of talc and graphite enriched in opaque minerals of chromite, sulphides and iron oxides (Fig.6c). The basaltic andesite rocks are composed of plagioclase and quartz embedded in fine matrix of plagioclase, hornblende, chlorite and quartz. Altered minerals of carbonates, sericite and chlorite are present along fractures. The dacitic rhyolite rocks are mainly composed of quartz, orthoclase and plagioclase phynocrysts embedded in very fine matrix of feldspar, quartz, sericite, and iron oxides. The quartz phynocrysts are stretched forming augen texture along the thrust zones (Fig.6d). The gabbro diorite rocks are composed of plagioclase and hornblende; sericite and chlorite present as altered minerals; quartz and opaques are accessory minerals. The mineral composition of the tonalite is mainly plagioclase, quartz and biotite. The sericite is altered mineral from plagioclase. Few opaque minerals are also present.

4.3.1. 2. Ore mineralogy

The ore microscopic study of the Barramiya gold mine revealed presence of chromian spinel, pyrite, arsenopyrite, chalcopyrite ore minerals and fine specks of gold in the talc graphite schist and listwaenite alterations (Figs. 7a, 7b& 7c). In area1, the ore mineral assemblages in the quartz veins and the listwaenite alterations are pyrite arsenopyrite and chalcopyrite. Fine specks of gold were recorded in the arsenopyrite in the quartz veins (Fig.8a), and fine disseminated gold along fractures in the listwaenites were also present (Fig.8b). In area 2, the quartz veins are enriched in pyrite, arsenopyrite and chalcopyrite hosting tiny specks of gold (Fig.8c). Fine disseminated specks of gold along fractures in the listwaenites were also recorded (Fig.8d).

4.3.1. 3. XRD analysis

The XRD analysis revealed peaks of gangue minerals of talc, quartz, calcite, ankerite and magnesite in both alteration zones (area 1 and area 2) (Figs 9a and 9b)

4.3.1. 4. SEM analysis

In area 1, the SEM investigation of the quartz veins revealed tiny specks of gold in the hosted arsenopyrite, its EDXA spot microanalysis showed presence of arsenopyrite, pyrite, nickel and magnetite minerals (Fig.10a). Fine rounded specks of disseminated gold were detected in the listwaenite alterations (Fig. 10b). In area 2, the SEM result of the quartz veins displayed pyrite and chalcopyrite host tiny specks of gold, its EDXA spot microanalysis illustrated ore minerals of pyrite, chalcopyrite and fine specks of gold (Fig.10c). The SEM of the listwaenite alterations, revealed arsenopyrite ore mineral host tiny specks of gold, its EDXA spot microanalysis displayed ore minerals of arsenopyrite, pyrite, magnetite and fine specks of gold (Fig. 10d).

4.3.2. Geochemistry

4.3.2.1. Fire assay analysis

In the Barramiya gold mine, the Fire assay for gold determined an average content for this metal in the graphite schist of 5.04 ppm. This is higher than its content in the quartz veins, which is 4.02 ppm and than in the listwaenites, which is 3.76 ppm (Table 2). The gold in the Barramiya mine is present in the talc graphite schist and quartz veins, as inclusions in sulphide ore minerals and as free disseminations in the fractures in the listwaenite alterations. The chromian spinel is a remnant of the host-rock and is present among the accessory minerals.

4.3.2.2. Atomic absorption analysis

In area 1, the atomic absorption analysis determined an Au average content in the quartz-veins of 2.4 ppm, an average Ag content of 8.0 ppm and a Cu average content of 2.4 wt%. Relatively higher averages of Au and Cu (up to 4.4 ppm and 2.8 wt% respectively) were recorded in the listwaenite alterations (Table 3). The Fire assay result proved presence of gold, (Table 4) that shows an average gold content of 2.9 ppm in the quartz veins and 1.5 ppm in the listwaenite alteration of area 1. The gold was recorded as fine specks in the arsenopyrite in the quartz veins and as fine disseminations along fractures in the listwaenite alterations.

In area 2, the atomic absorption analysis determined in the quartz-veins an Au average content of 2.6 ppm, an Ag average content of 6.2 ppm and Cu average of 1.9 wt%. In the listwaenite alteration, relatively higher averages of Au (3.5 ppm) and Cu (2.4 wt %) were recorded (Table 5). Also, the Fire assay result confirmed presence of gold, (Table 6) that shows an average gold content of 3.1 ppm in the quartz veins and 1.7ppm in the listwaenite alteration.

5. Discussion:

The origin of gold in the Eastern Desert of Egypt is a matter of controversy. Hume (1937) assumed that gold mineralization is an integral part of one surge of mineralization connected with hydrothermal activities related to diorite intrusions of the Proterozoic age. From this point of view, the Barramiya ultramafics must have been intruded from the south and the east by gabbro-diorite associated with hydrothermal gold-bearing solutions ascending along fractures and along the thrust fault contacts of the ultramafics and metavolcanics to constitute the gold-bearing alteration zones. These hydrothermal solutions also impregnated stocks of quartz veins and silicified iron carbonate (listwaenite ridges) to enrich them in the gold that was analytically detected by our study in such loads and stocks. El-Shazly (1957) considered that gold mineralization is multi-aged and mostly related either to the Gattarian granites (a type locality at Gabal Gattar area northern eastern desert of younger granite) or due to many tectonic magmatic stages ranging from the geosynclinal to the platform stage. This hypothesis may be applied to the Barramiya ultramafics, which are intruded from the north by tonalite intrusions that act as a source for a later phase of hydrothermal fluids, which precipitated sulphides and gold in loads and stocks of quartz veins and silicified carbonated listwaenite alterations. Buisson and Leblanc (1987) proposed a model in which ultramafic rocks of the ophiolitic complexes acted as a source where gold was leached and concentrated during serpentinization of the ophiolitic ultramafic rocks. This model is alsol applicable to the Barramyia area, where the huge carbonate-rich ultramafics provided gold during the processes of serpentinization, graphitization and listwaenitization. Murr (1999) proposed two different stages of mineralization. During the first stage, a chemical reaction of a fluid (pH between 3.5 and 5) with the host rock can be assumed, resulting in the formation of sericite and quartz. If gold was transported as a sulphide complex in the reactive fluid, primary iron from the host rock and sulphide from the fluid could have formed pyrite while the gold was being precipitated. Gold was confined within this first stage of mineralization mainly to pyrite or arsenopyrite. The second stage of mineralization can be observed within the quartz veins. The main minerals are pyrite, sphalerite, galena and chalcopyrite, with minor amounts of digenite, hessite, calaverite, scheelite, hematite and tetrahedrite. In the Barramiya area, the gold occurs within quartz, listwaenite arsenopyrite and pyrite ore minerals. Taylor and El-Kazzaz (2002) remarked that gold-mineralized quartz vein systems in the Wadi Allaqi in the South Eastern Desert were emplaced along syn-kinematic D1 shear zones. This situation may be similar to the Barramiya area, in which the gold-bearing listwaenite alterations and quartz veins are developed along the fractures and thrust contacts between ultramafics and metavolcanic rocks. Gold and sulfur were leached from listwaenite by dilute aqueous-carbonic fluids. Au deposition was trigged by pressure fluctuation and sharp decrease in fluid fO_2, Zoheir and Lihman (2011).

6. Conclusion

In the present study, the use of ASTER data and extensive field work undertaken enables to detect two hydrothermal alteration zones (area1 and area 2) of high gold mineralization in the Barramiya district. The band ratios derived from the image spectra and the spectral unmixing method based on n-dimensional spectral feature space has been developed and validated through field verification of the studied district. ASTER data evaluation shows good correlation with the geological field observations and geochemical investigations of collected samples. VNIR and SWIR relative reflectance spectral analysis was accurate and helpful for detecting and mapping mineral alteration zones. Mineralogical information on the alteration zones obtained by ASTER surface data indicates that the Barramiya district has good potential for further gold exploration because of the existence of extensive and intense alteration zones in the study area.

The interpretation of the field observations, mineralogical investigation and geochemical analyses illustrated the paragensis of the rocks related to the mineralized alteration zones in the Barrmiya district. The paragenesis includes the following; in the first stage, the essential minerals such as olivine, pyroxene, antigorite and chrysotile were directly separated and crystallized from the magma forming the ultramafic and mafic rocks of the area. During this stage post-magmatic fluids were circulating and were connected along the fractures, fault planes and shear zones in the surrounding and adjacent rocks. The second stage includes the deposition of the magmatic fluids forming altered and accessory minerals as talc calcite, ankerite, dolomite, magnesite, opaque minerals and quartz. The third stage corresponds to the mineralization phase in which the ore mineral assemblages such as the association of pyrite, chalcopyrite arsenopyrite, gold and Cu, together with free gold disseminations were formed. This ore mineralization is accompanied by chloritization and carbonitization processes.

The ASTER images prove to be a powerful tool in the initial steps of mineral exploration because they provide high accuracy data that can be used as a basis for mapping the surface distribution of certain minerals. In this way they allow the determination of hydrothermal alteration zones, reducing the time and coast required for field exploration and evaluation.

Acknowledgements

Great thanks are due to the Deutsche Forschungsgemeinschaft (DFG), Germany for funding this work. Many thanks to NARSS and the Karlsruhe Institute of Technology for their Additional support. The authors also, would like to thank Prof. Dr Ibrahim El Kassas, NARSS for his sincere help and discussions.

References:

Abdelsalam, M. and Stern, R.J., 1996. Sutures and shear zones in the Arabian Nubian Shield, Journal of African Earth Sciences, 23, 289-310.

Abrams, M.J.; Ashley, R.P.; Rowan, L.C.; Goetz, A.F.H and Khale, A.B., 1977. Mapping of hydrothermal alteration in Cuprite mining district, Nevada, using aircraft scanner images for the spectral region 0.46 to 2.34 mm. Geology, 5, 713–718.

Abrams, M.J.; Brown, D.; Leple, L. and Sadowski, R., 1983. Remote sensing of porphyry copper deposits in Southern Arizona, Econ. Geol., 78, 591–604

Abrams, M., Hook, S.J., 1995. Simulated ASTER data for geologic studies. IEEE Trans. Geosci. Remote. Sens. 33 (3).

Agar 1992. The tectono-metallogenic evolution of the Arabian Shield, Precambrian Research, 58, 169-194.

Ali-Bik, Taman, El Kalioubi, B., Abdel Wahab, 2012. Serpentinite-hosted talc-magnesite deposits of Wadi Barramiya area, Eastern Desert, Egypt: characteristics, petrogenesis and evolution. Journal of African Earth Sciences 64, 77–89.

Al Shanti, A. M. S.; Frisch, W.; Pohl, W. and Abdel Tawab, M.M., 1978. Precambrian Ore deposits in the Nubian and the Arabian shields and their correlation across the Red Sea.Österr. Akad. Wiss. Schriftenr. Erdwiss. Komm, 3, 37-44.

Amin, M.S., 1955. Geological Features of Some Mineral Deposits in Egypt, Bull. Inst. Desert D'Egypte, 5, 209-240.

Attia, M. I., 1948. Geology of Barramiya mining district. Geological Survey of Egypt, Governmental Press, Cairo.

Azizi, H.; Rasouli, A.A. and Babaei, K., 2007. Using SWIR bands from ASTER for discrimination of hydrothermal altered mineral in the northwest of Iran (SE Sanadaj city); a key for exploration of copper and gold mineralization. Res. J. Appl. Sci., 2, 763–768.

Blasband, B.; White, S.; Brooijmans, P.; De Boorder, H. and Visser, W., 2000. Late Proterozoic extensional collapse in the Arabian- Nubian Shield. Journal of Geological Society of London, 157, 615-628.

Boardman, J.W., Kruse, F.A., Green, R.O., 1995. Mapping target signatures via partial unmixing of AVIRIS data. In: Green, R.O. (Ed.), Summaries of the Fifth JPL Airborne Earth Science Workshop, JPL Publication 95-1, Pasadena, CA, 1, 23-26.

Botros, N. Sh., 2004. A new classification of the gold deposits in Egypt. Ore Geology Reviews, 25, 1-37.

Buisson, G. and Leblanc, M., 1987. Gold in mantle peridotites from Upper Proterozoic ophiolites in Arabia, Mali, and Morocco. Economic Geology, 82, 2091-2097.

Burke, K. and Sengör, C., 1986. Tectonic escape in the evolution of the continental crust, AGU Geodynamic, Ser. 14, 41-53.

Crosta, A.P.; De Sousa, F.; Azevedo, C. and Brodie, F., 2003. Targeting key alteration minerals in epithermal deposits in Patagonia, Argentina, using ASTER imagery and principal component analysis. Int. J. Remote Sens., 24, 4233–4240.

Delfour, J., 1980. Geologic, tectonic and metallogenic evolution of the northern part of the Precambrian Arabian shield (Kingdom of Saudi Arabia), Bull. BRMG 11/1-2, 1-20, Orleans.

Di Tommaso and Rubinstein, 2007. Hydrothermal alteration mapping using ASTER data in the Infiernillo porphyry deposit, Argentina. Ore Geology Reviews, 32, 275-290.

EGSMA, 1992. Geologic map of Wadi Al Barramiyah Quadrangle, Egypt. Scale 1:250 000. Egyptian Geological Survey and Mining Authority, Cairo, Egypt.

EGSMA, 2000. Geologic map of Wadi Al Barramiyah Quadrangle, Egypt. Scale 1:100 000. Egyptian Geological Survey and Mining Authority, Cairo, Egypt.

El-Alfy, E., 1946. Mineral Resources of Egypt. Trans. Min. Petroleum Assoc., Egypt, 1, 3, 9-32.

El-Ramly, M. F.; Ivanov, S.S and Kochin, G. G., 1970. The Occurrence of Gold in the Eastern Desert of Egypt. Article 4 in Studies on some Mineral Deposits of Egypt, Edited by O. Moharram et al. Geological Survey of Egypt, Cairo, Egypt, 53-64.

El Shafei, S.; Megahid, A. and EL Sherif, M., 1983. Processing of Barramiya h gold ores, Egypt, using heap-leach method. Journal of African Earth Science, 34, 263- 266.

El Shazly, E.M., 1957. Classification of the Egyptian mineral deposits, Egypt. Journal of Geology, 1, 1-20.

El-Shazaly, E. M., 1959. Notes on the Mining Map of Egypt. Proceedings of the 20th International Geological Congress (1956), Mexico, Assoc. African Geological Surveys, 423-437.

El-Zoghby, M.E., 1953. The Mineral Resources of Egypt. Trans. Min. Petroleum Association Egypt, 8, 3,137-158.

Farrand,W.H., Harsanyi, J.C., 1997. Mapping the distribution of mine tailings in the Coeur d'Alene River Valley, Idaho, through the use of a constrained energy minimization technique. Remote Sensing of Environment 59 (1), 64-76.

Gad, S. and Kusky, T. M, 2006. Lithological mapping in the Eastern Desert of Egypt, the Barramiya area, using Landsat Thematic Mapper (TM). Journal of African Earth Science, 44, 196-202.

601 Galvao, L.S.; Filho, R.A., and Vitorello, I., 2005. Use of ASTER short-wave infrared bands for the spectral discrimination of hydrothermally altered-materials, Central Mexico. Int. J. Remote Sens, 19, 1981–2000.

604 Garson, M. and Shalaby, I.M., 1976. Precambrian-Lower Paleozoic plate tectonics and metallogenesis in the Red Sea region. Special Paper of the Geological Association of Canada, Ontario, 14, 573-596.

607 Garven, G.; Appold, M. S.; Toptygina, V. I. and Hazlett, T. J., 1999. Hydrogeologic modeling of the genesis of carbonate-hosted lead-zinc ores, Journal of Hydrogeology, 7, 108-126.

609 Gass, I.G., 1982. Upper Proterozoic Pan African calcalkaline magmatism in northeastern Africa and Arabia. In: R.S. Thorpe, Editor, Wiley, New York, 591-609.

611 Gillespie, A. R., Matsunaga, T, Rokugawa, S., & Hook, S. J. 1998. Temperature and Emissivity from Advanced Spaceborne Thermal Emission and Reflection Radiometer (ASTER) images. IEEE Transactions on Geoscience and Remote Sensing, 36, 1113-1126.

614 Goetz, A.F.H.; Rock, B.N., and Rowan, L.C., 1983. Remote sensing for exploration, an overview. Econ. Geol., 78, 573–590.

616 Goldfarb, R.J.; Groves, D.J. and Gardoll, S., 2001. Orogenic gold and geologic time a global synthesis. Ore Geology Reviews, 18, 1-75.

618 Green, A. A., Berman, M., Switzer, B., & Craig, M. D. (1988). A transformation for ordering multispectral data in terms of image quality with implications forjibisefrernoval. IEEE Transactions on Geoscience and Remote Sensing, 2, 6(1), 65-74

621 Greiling, R.O.; Abdeen, M.M.; Dardir, A.A.; El-Akhal, H.; El-Ramly, M.F.; Kamal, G.M. El-Din.; A.F., Osman.; A.A. Rashwan.; A.H., Rice, N. and Sadek, M.F., 1994. A structural synthesis of Proterozoic Arabian Shield in Egypt. Geologische Rundschau, 83, 484- 501.

624 Groves, D.L.; Goldfarb, R.J.; Gebre-Mariam, M.; Hagemann, S.G. and Robert, F., 1998. Orogenic gold deposits: a proposed classification in the context of their crustal distribution and relationship to other gold deposit types. Ore Geology Reviews, 13, 7-27.

627 Groves, D.I.; Goldfarb, R.J.; Robert, F. and Hart, C.J.R., 2003. Gold deposits in metamorphic belts: overview of current understanding, outstanding problems, future research, and exploration significance. Economic Geology, 98, 1-29.

630 Hannington, M.D.; Poulse, K.H.; Thompson, J.F.H. and Sillitoe, R.H., 1998. Volcanogenic gold in the massive sulphide environment. In: Barrie, C.T. and Hannington, M.D. (Eds.), Volcanic-Associated Massive Sulphide Deposits: Processes and Examples in Modern and Ancient Settings. Reviews in Economic Geology, 8, 325-35.

Harraz, H.Z., 1999. Wall rock alteration, Atud gold mine, Eastern Desert, Egypt: processes and P–T-X CO2 conditions of metasomatism. Journal African Earth Sciences, 20, 527-551.

Harsanyi,J.C., and Chang, C.L, 1994. Detection of subpixel signatures in hyperspectral image sequences. In: Lyon, J. (Ed.), Proc. American Society for Photogrammetry and Remote Sensing (ASPRS) Annual Meeting, Reno, Nevada, 236-247.

Hume,W. F., 1907. A preliminary report on the Geology of the eastern desert of Egypt. Survey Department, National print. Cairo, Egypt, 72.

Hume,W.F., 1934. The fundamental Pre-Cambrian rocks of Egypt and the Sudan, their distribution, age and character, the metamorphic rocks. Geology of Egypt, 2, Part 1, Survey of Egypt, Government Press, Cairo.1-300.

Hume, W.F., 1937. The fundamental Pre-Cambrian rocks of Egypt and the Sudan, their distribution, age and character, the minerals of economic value associated with the intrusive Precambrian igneous rocks. Geology of Egypt. 2, Part 3, Survey of Egypt, Government Press, Cairo. 689-990.

Hussein, A. A., 1990. Mineral Deposits. In: The Geology of Egypt, Edited by R. Said. A. A. Balkema, Rolterdam/ Brook field, 511- 566.

Ibrahim, M. M., 1942. Report on Barramiya District, Egypt. Geological Survey of Egypt, Cairo, Egypt.

Jackson, N.J., 1986. Mineralization associated with felsic plutonic rocks in the Arabian Shield. Journal of African Earth Science, 4, 213-227.

Johnson, P.R. and Woldehaimanot, B., 2003. Development of the Arabian Nubian Shield: perspectives on the accretion and deformation in the northern East African Orogen and the assembly of Gondwana. In: Yoshida, M., Windley, B.F., Dasgupta, S. (Eds.), Proterozoic East Gondwana: Supercontinent Assembly and Break-up. Geological Society of London, Special Publication, 289-325.

Johnson, P.R., Andresen, A., Collins, A.S., Fowler, A.R., Fritz, H., Ghebreab, W., Kusky, T.,Stern, R.J., 2011.Late Cryogenian–Ediacaran history of the Arabian–Nubian Shield: a review of depositional, plutonic, structural, and tectonic events in the closing stages of the northern East African Orogen. Journal of African Earth Sciences 61, 167–232.

Kaufmann, H., 1988. Mineral exploration along the Aqaba-Levant structure by use of TM- data: Concepts, processing and results. International Journal of Remote Sensing, 10, 1639-1658.

Kerrich, R., Fyfe, W.S., 1981. The gold–carbonate association: source of CO2 and CO2 fixation reactions in Arcean lode deposits. Chem.Geol. 33, 265–294

Kesler, S.E.; Chryssoulis, S.L. and Simon, G., 2002. Gold in porphyry copper deposits: its abundance and fate. Ore Geology Reviews, 21, 103-124.

Kochin, G. G. and Bassiuni, F. A., 1968. The Mineral Resources of the UAR, Part I: Metallic Minerals. Internal Report No. 18/68, Geological Survey of Egypt, Cairo, Egypt.

Kröner, A.; Krüger, J. and Rashwan A. A., 1994. Age and tectonic setting of granitoid gneisses in the Eastern Desert of Egypt and south-west Sinai, Geol. Rundsch., 83, 502-513.

Kruse, F.A.; Lefkoff, A.B.; Boardman, J.W.; Heidebrecht, K.B.; Shapiro, A.T.; Barloon, P.J. and Goetz,A.F.H.,1993.The spectral image processing system (SIPS)–interactive visualization and analysis of imaging spectrometer data. Remote Sens. Environ 44,145–163.

Langwieder,G.,1994. Die Geologie des Gebietes Wadi El-Sid/Um El Fawakhir und Geochemische Untersuchungen an Quarzgängen des gold lagerstättenbezirkes El Sid/Fawakhir. Unpublished M.Sc. Thesis, Ludwig-Maximilians-Universität München,122.

Mansour, M.S.; Bassuni, F. A. and Al-Far, D. M., 1956. Geology of Umm Salatit-El Hisinat district (Barramiya h East sheet), unpublished report No.2249 Geol. Surv. Cairo,Egypt.

Mars, J.C., Rowan, L.C., 2006. Regional mapping of phyllic- and argillic-altered rocks in the Zagros magmatic arc, Iran, using Advanced Spaceborne Thermal Emission and Reflection Radiometer (ASTER) data and logical operator algorithms. Geosphere 2, 161-186.

Murr, A., 1999. Die Genese der Goldlagerstättenbezirke Fatira, Gidami, Atalla and Hangaliya in der Ägyptischen Ostwüste, Münchner Geol. Hefte, A. 27, 202.

Nesbitt, B.E., 1992. Orogeny, crustal hydrogeology and the generation of epigenetic ore deposits in the Canadian Cordillera. Mineralogy and Petrology, 45, 153-179.

Oliver, J., 1986. Fluids expelled horizontally from orogenic belts: Their role in hydrocarbon migration and other geologic phenomena. Geology, 14, 99-102.

Podwysocki, M.H.; Segal, D.B. and Abrams, M.J.,1983. Use of multispectral images for assessment of hydrothermal alteration in the Marysvale, Utah mining area, Econ. Geol., 78, 675–687.

Phillips, G.N., Brown, J.J., 1987. Host rock and fluid control on carbonate assemblages in the Golden Mile dolerite, Kalgoolie gold deposit, Australia. Can. Mineral. 25, 265–273.

Pohl, W., 1979. Metallogenic, Menerogenic analyses contribution to the differentiation between Mozambiquian basement and Pan-African superstructure in the Red Sea region. Ann.Geol. Survey Egypt, 9, 32-44.

Pohl, W., 1984. Large-scale metallogenic features of the Precambrian in the North- East Africa and Arabia. Bull. Fac. Earth Sci., King Abdelaziz University, 6, 591-601.

Pohl, W., 1988. Precambrian Metallogeny in NE Africa. In: El Gaby, S. and Greiling, R.O. (eds). The Pan-African of northeast Africa and adjacent areas. Braunschweig (Viewg) 319-341.

Roberts, D.A., Yamaguchi, Y., Lyon, R.J.P., 1986. Comparison of Various Techniques for Calibration of AIS Data in Proceedings, 2nd AIS Workshop. JPL Publication, vol. 86-35. Jet Propulsion Laboratory, Pasadena, California, 21-30.

Rowan, L. C., Wetlaufer, P. H., Goetz, A. F. H., Billlingsley, F. C., & Stewart, J. H.1974. Discrimination of rock types and detection of hydrothermally altered areas in south-central Nevada U.S. Geological Survey Professional Paper, 883, 35.

Rowan, L.C., Mars, J.C., 2003. Lithologic mapping in the Mountain Pass, California area using Advanced Spaceborne Emission and Reflection Radiometer (ASTER) data. Remote Sensing of Environment 84 (3), 350-366.

Sabet, A. H. and Zaatout, M. A., 1955. Geology of El-Shalul-El Bakriya District (Barramiya West Sheet). Geological survey of Egypt, Cairo, Egypt.

Safwat Gabr, Abduwasit Ghulam, T.M. Kusky, 2010. Detecting areas of high-potential gold mineralization using ASTER data Original Ore Geology Reviews, 38,59-69.

Sillitoe, R. H., 1979. Metallogenic consequences of late Precambrian suturing in Arabia, Egypt, Sudan and Iran. Bull. Fac. Earth Sci., 3/1, 110-120.

Stern, R.J., 1994. Arc assembly and continental collision in the Neoproterozoic East African Orogen: implication for the consolidation of Gondwanaland, Ann. Rev. Earth Planet. Sci., 22, 319-351.

Sultan, M., Arvidson, R.E., Sturchio, N.C., 1986. Mapping of serpentinites in the Eastern Desert of Egypt using Landsat Thematic Mapper data. Geology 14, 995-999.

Taylor, W.E.G. and El Kazzaz, Y.A., 2002. On the genesis of the shear-zone-hosted gold mineralization in South Eastern Desert, Egypt. Proceedings of the Cumberland Geological Society, 6, 540-552.

Van Der Meer, F., 1999. Imaging spectrometry for geological remote sensing, Geol. Mijnbouw., 77, 137–151.

Wallbrecher E. H.; Fritz, A.A.; Khudeir, H. and Farahad, F., 1993. Kinematics of Panafrican thrusting and extension in Egypt. In: U. Thorweihe and H. Schandelmeier, Editors, Geoscientific Research in Northeast Africa, Balkema, Rotterdam, 27-30.

Yamaguchi, Y., Naito, C., 2003. Spectral indices for lithologic discrimination and mapping by using the ASTER SWIR bands. Int. J. Remote. Sens. 24 (22), 4311-

Zierenberg, R.; Koski, R.; Morton, J.; Bouse, R. and Shanks, W., 1993. Genesis of massive sulphide deposits on a sediment-covered spreading centre, Escanaba Trough, Southern Gorda Ridge. Economic Geology, 88, 2069-2098.

Zoheir B, Lehmann B (2011). Listvenite-lode association at the Barramiya gold mine, Eastern Desert, Egypt. Ore Geology Reviews, 39, 101-115.

fig.1

Click here to download high resolution image

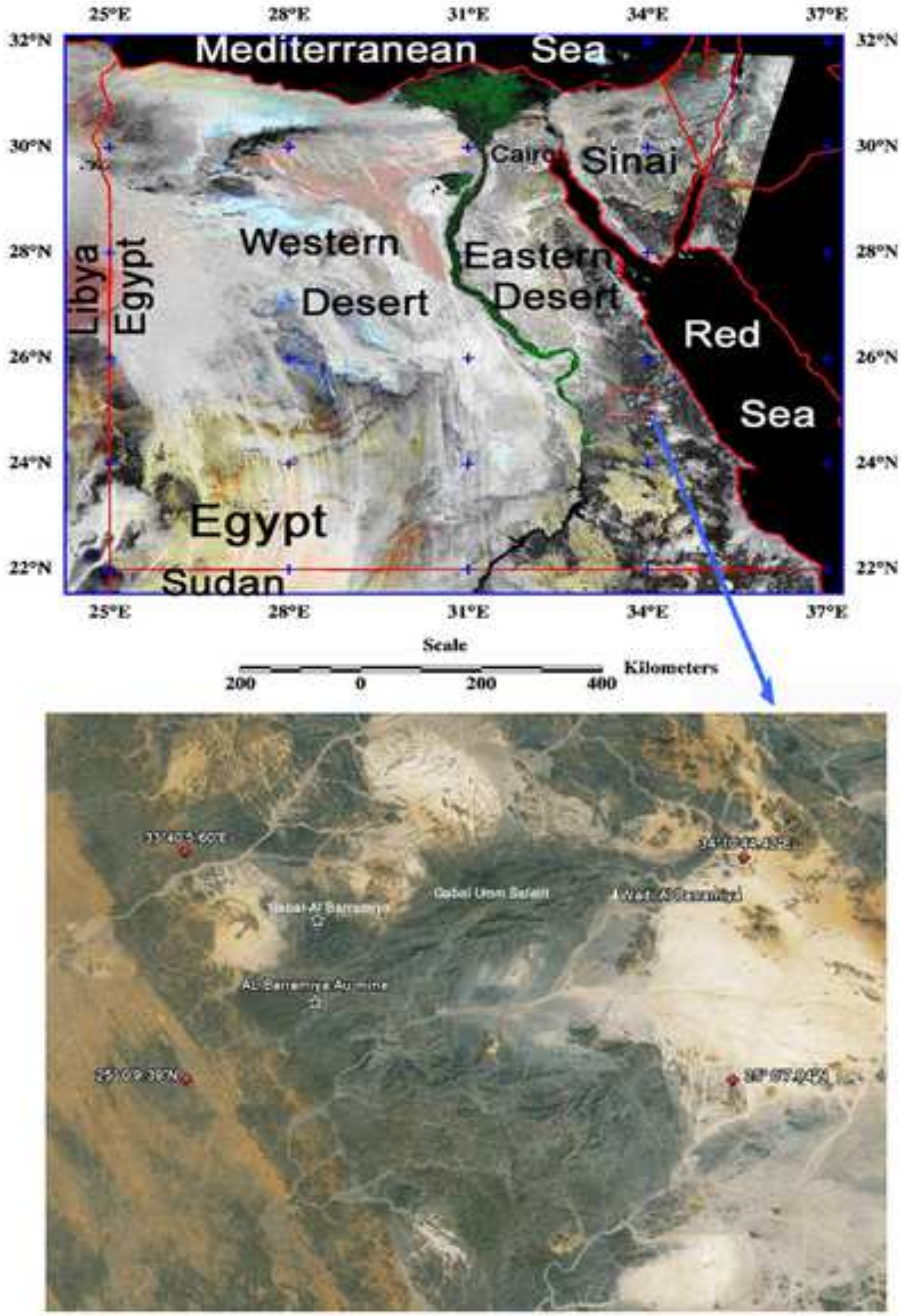

fig.2

Click here to download high resolution image

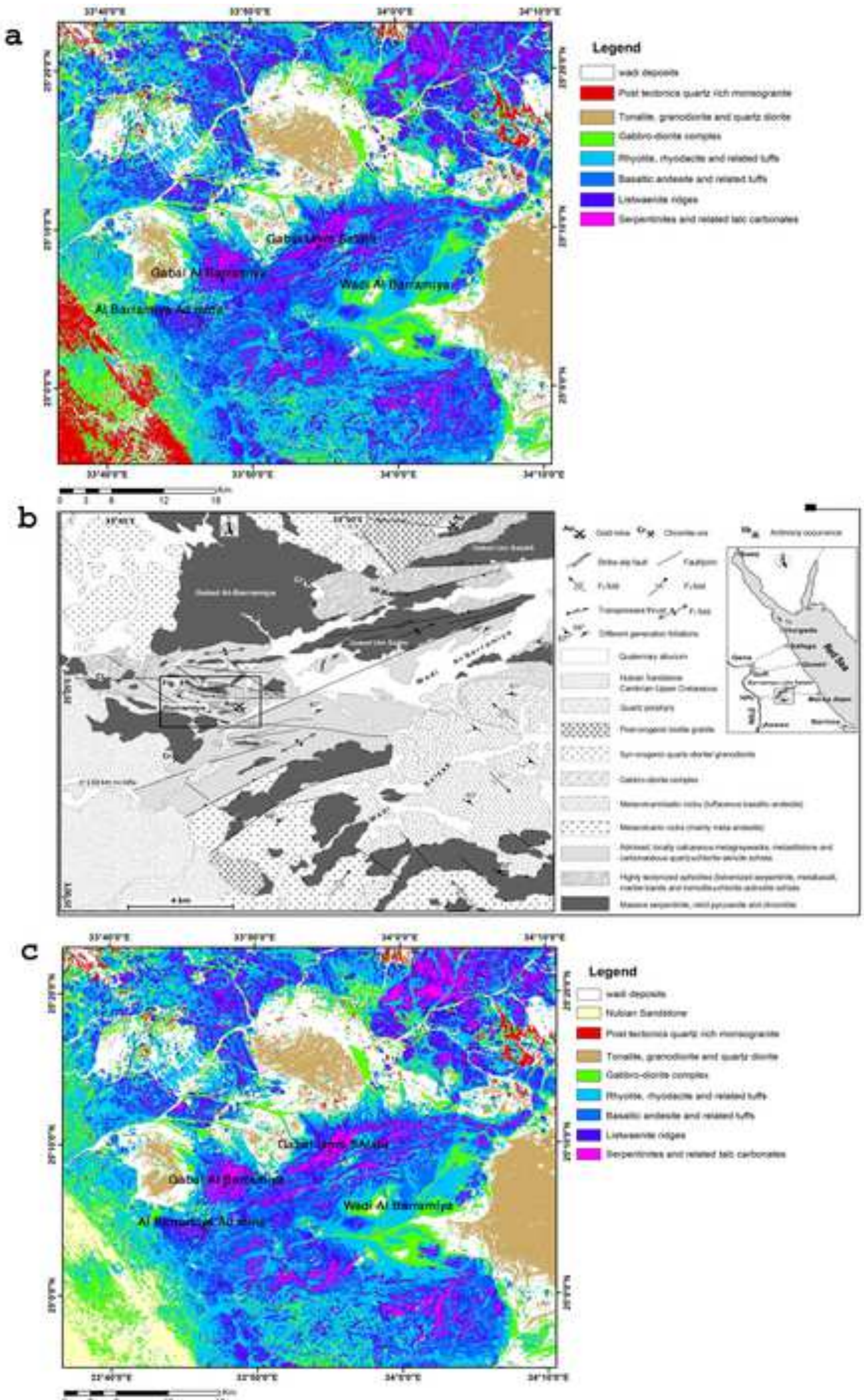

fig.3
Click here to download high resolution image

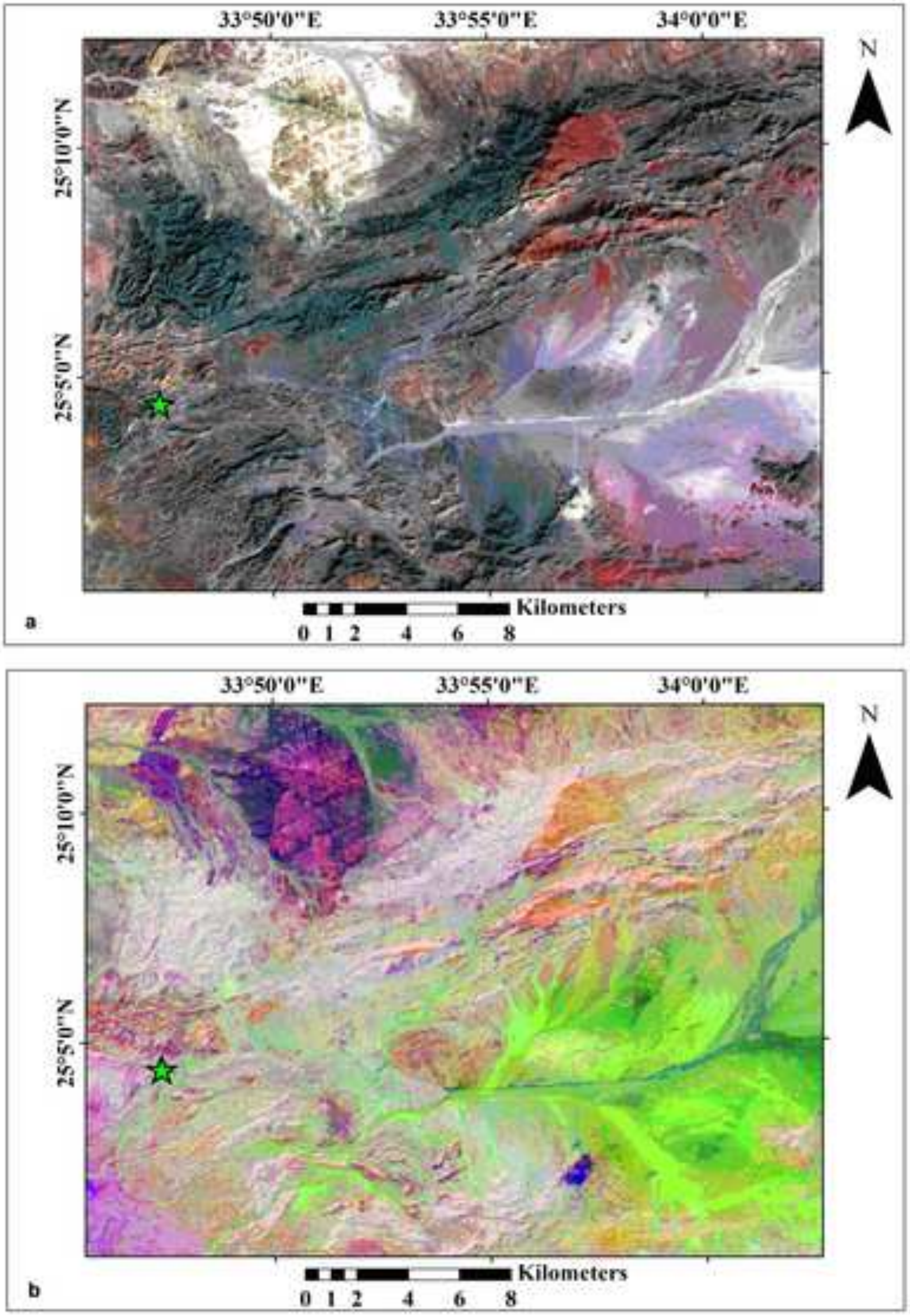

fig.3

Click here to download high resolution image

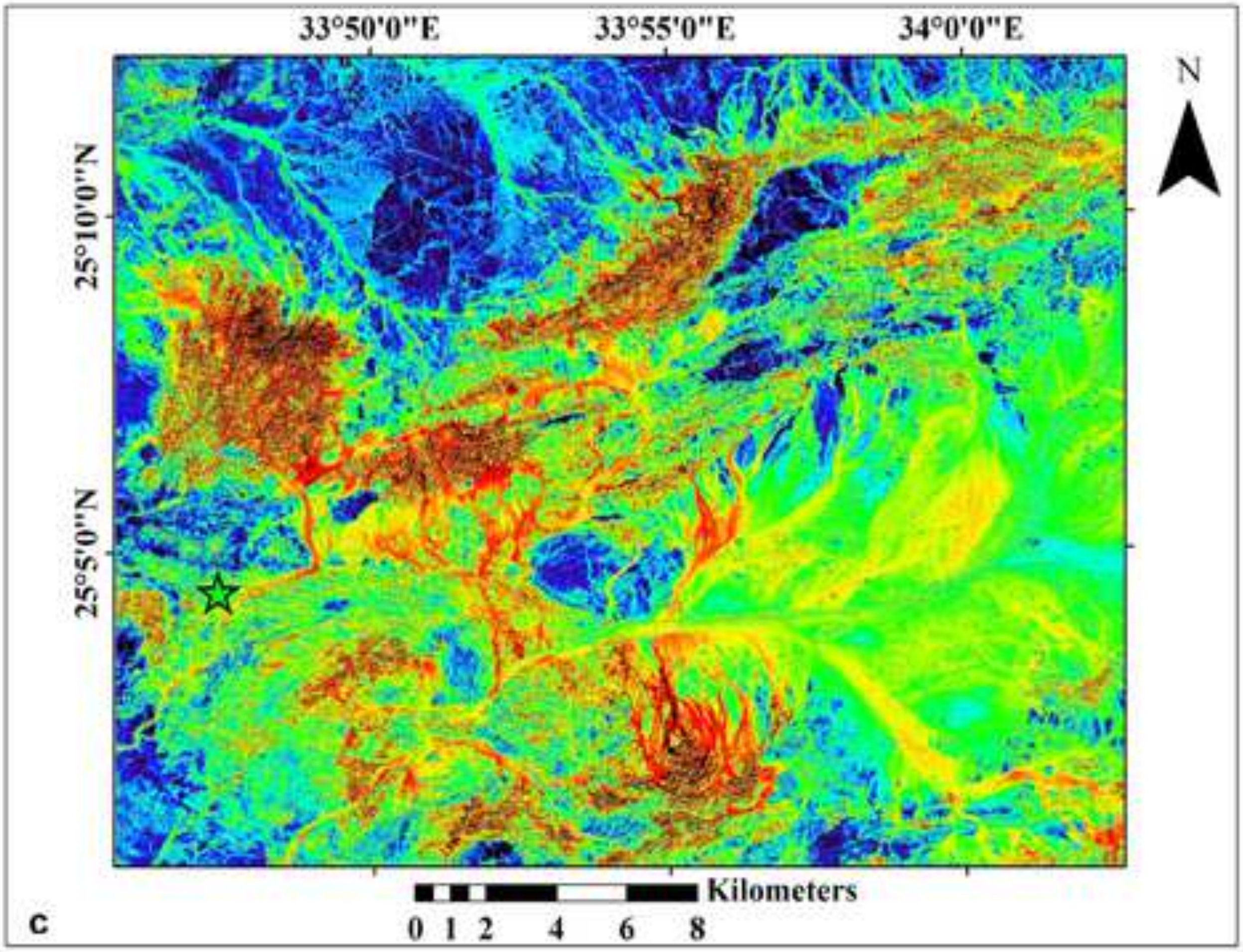

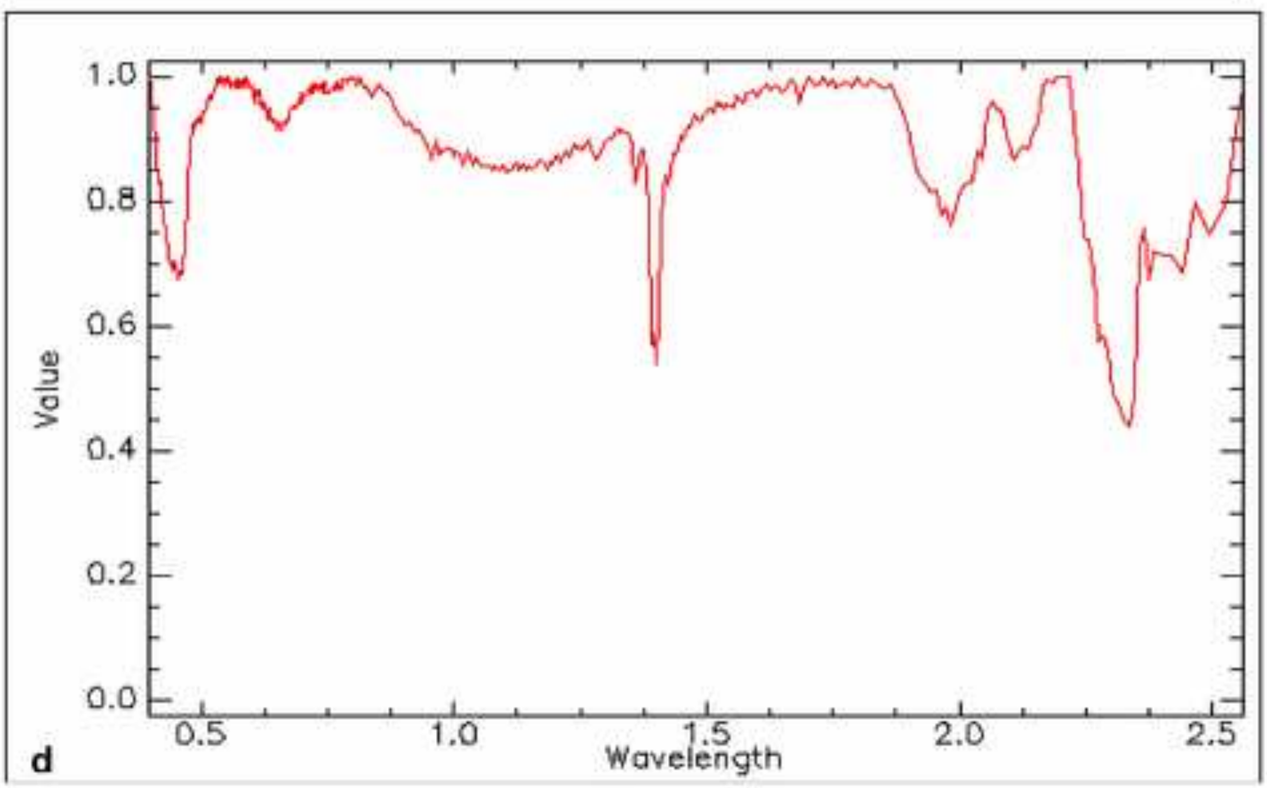

fig.3

Click here to download high resolution image

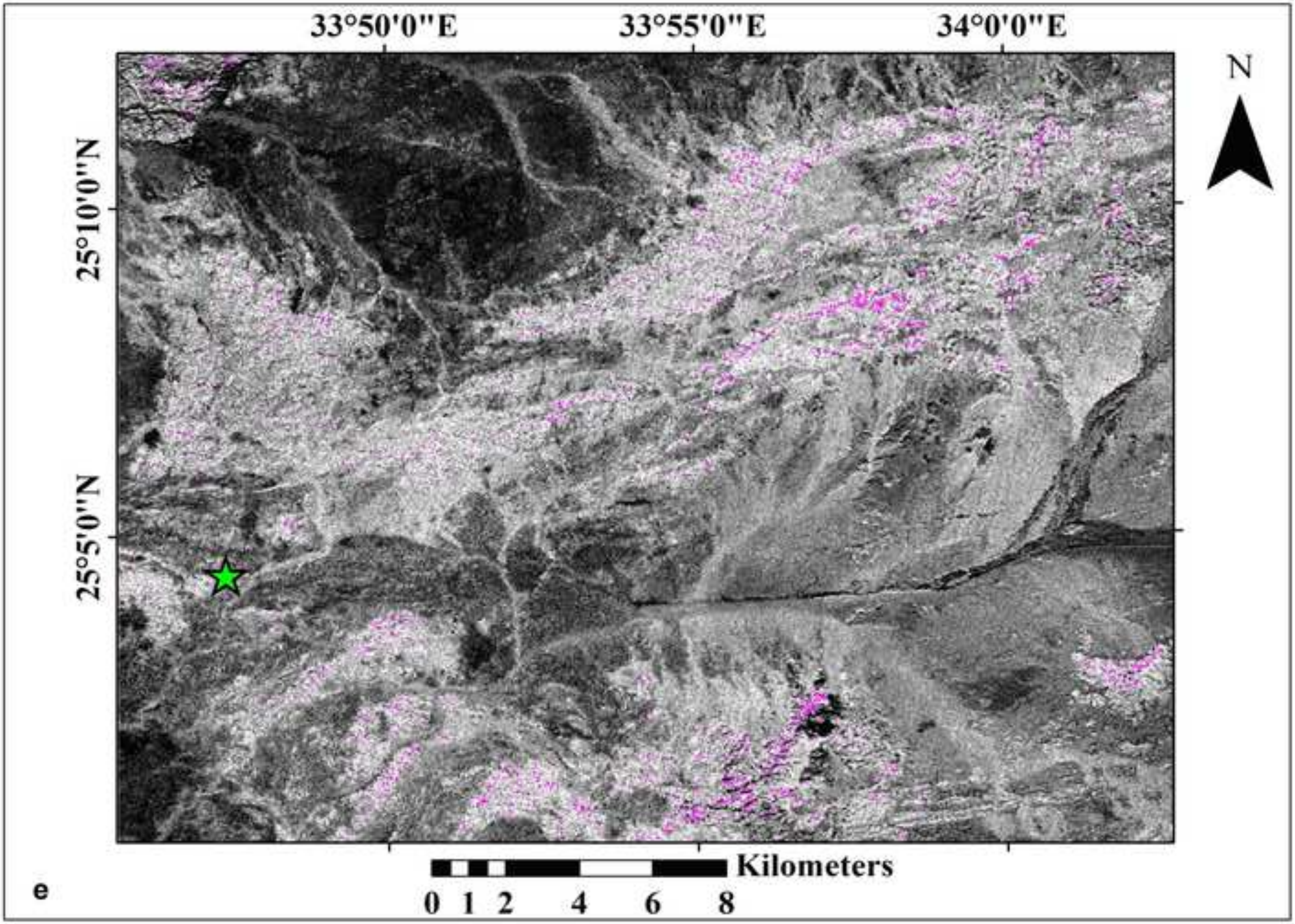

fig.3

Click here to download high resolution image

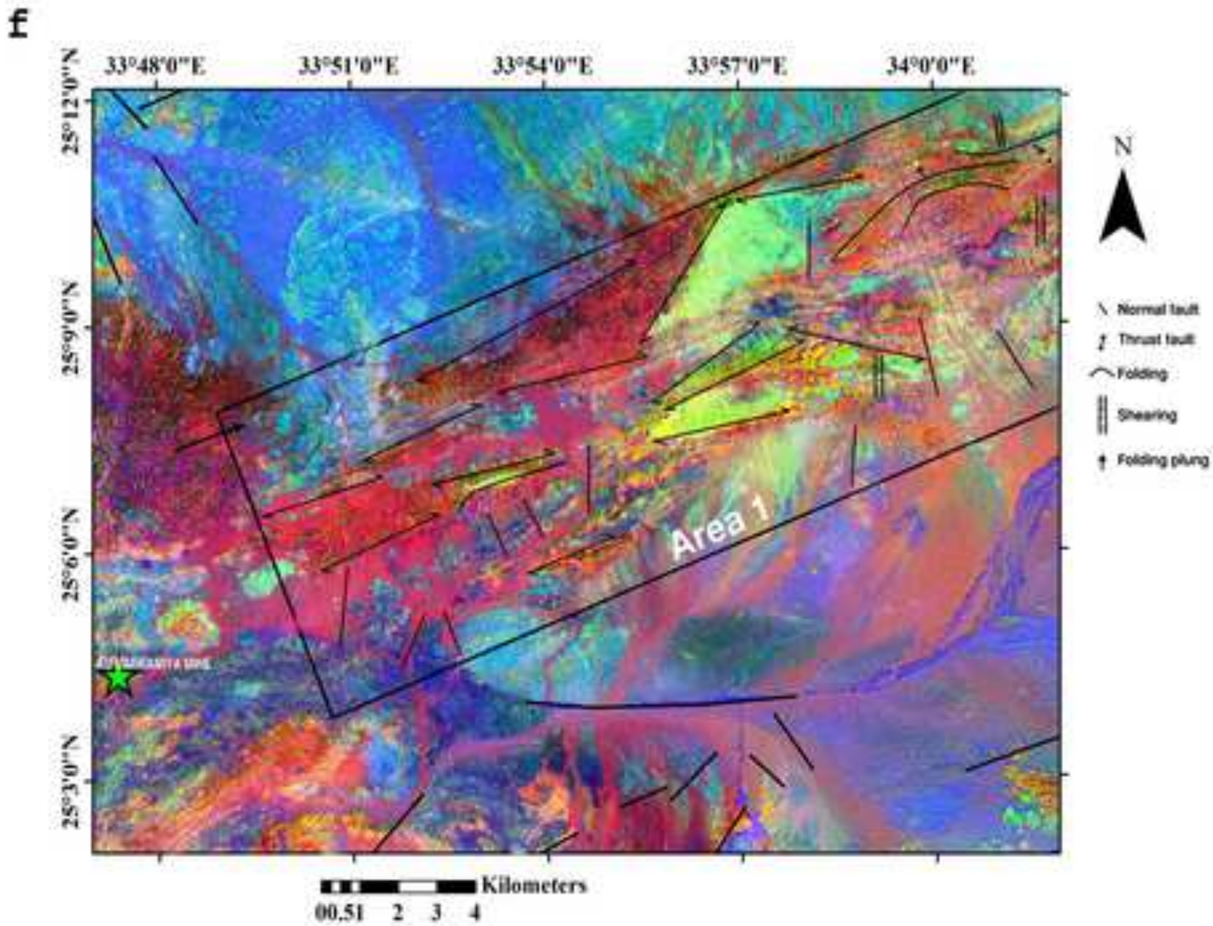

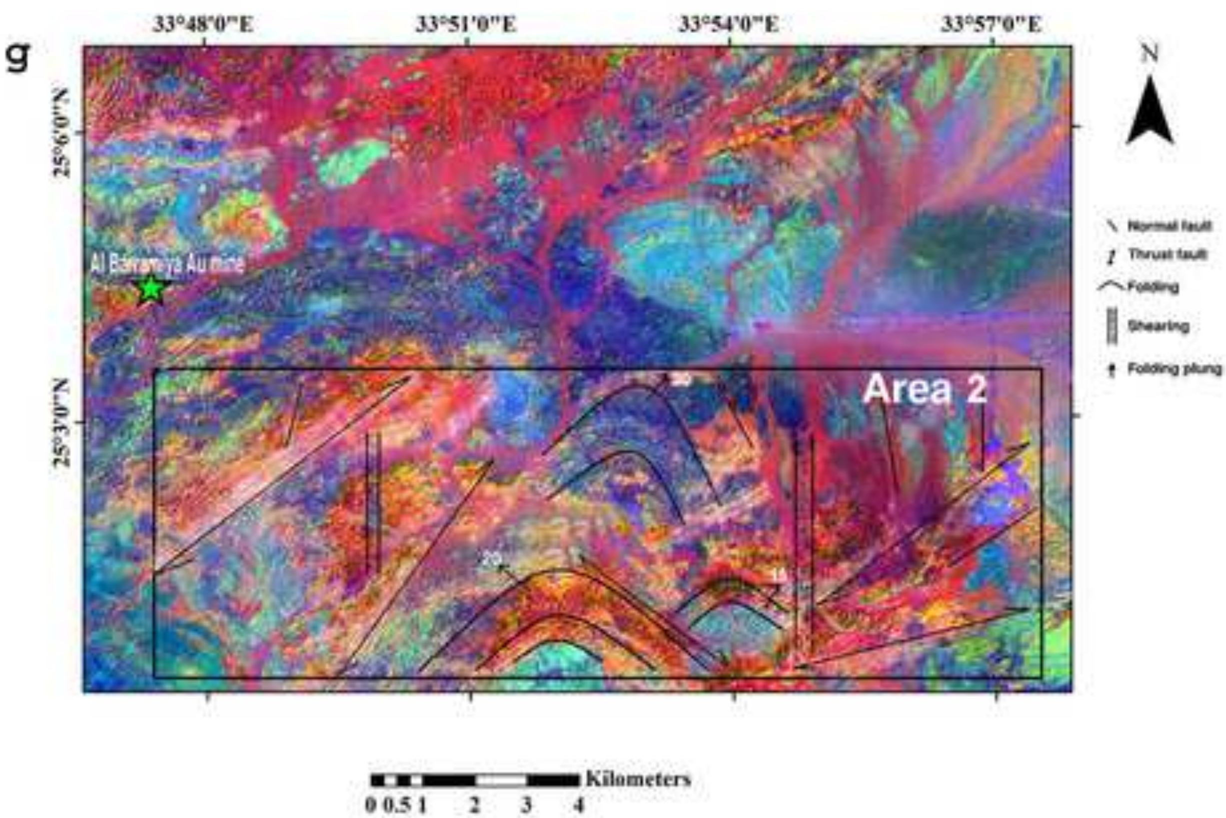

fig.4
Click here to download high resolution image

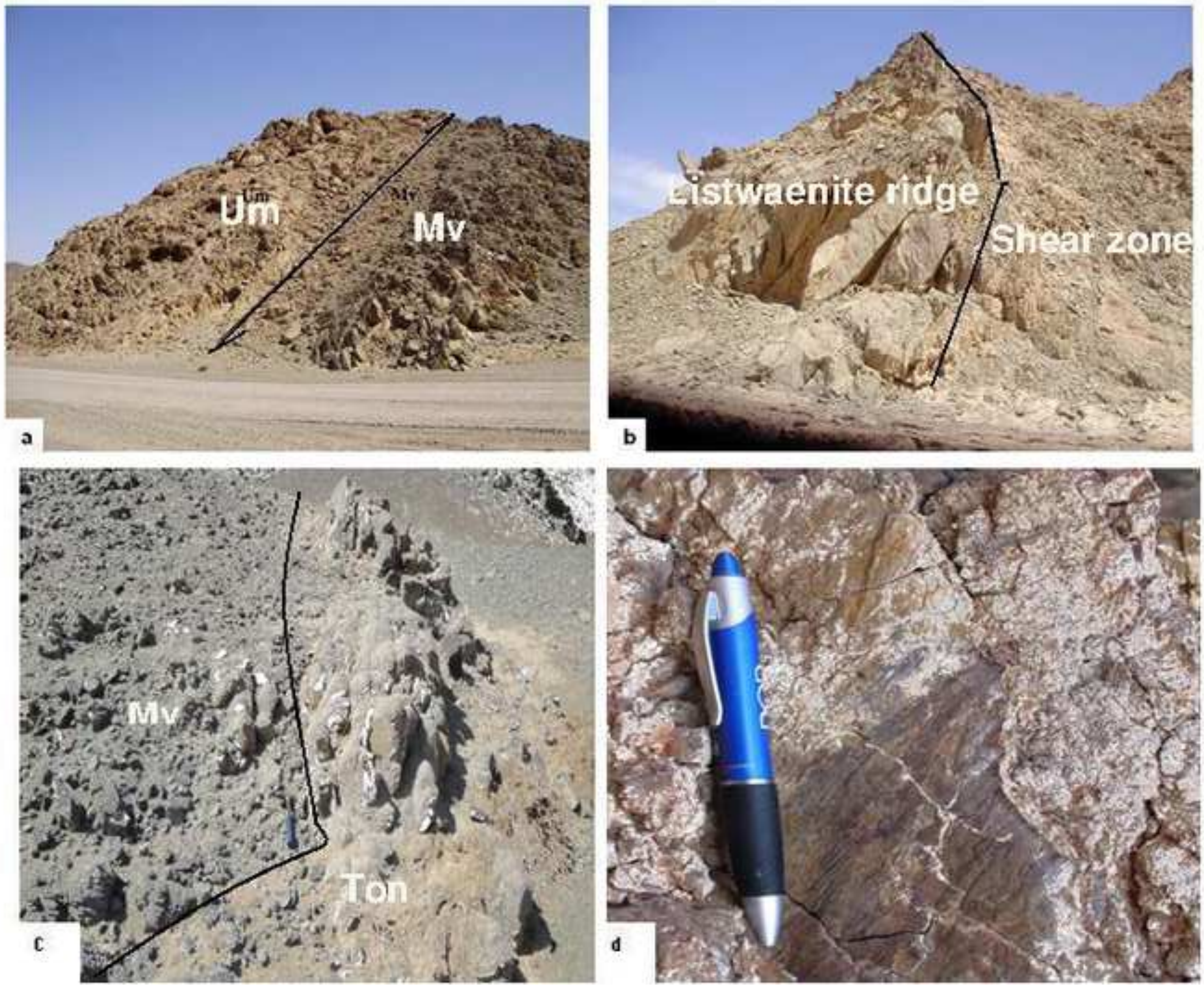

fig.5

Click here to download high resolution image

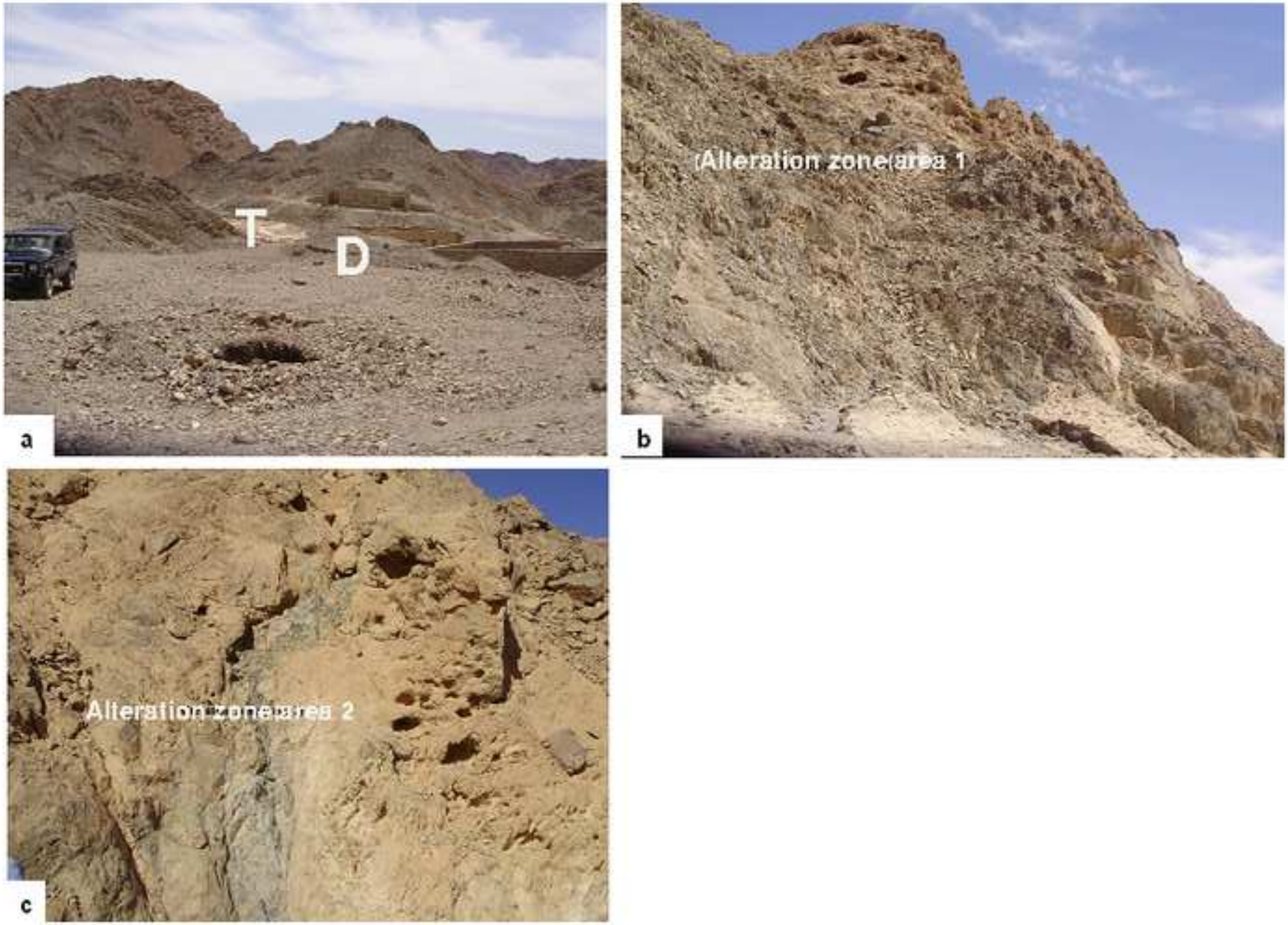

fig.6

Click here to download high resolution image

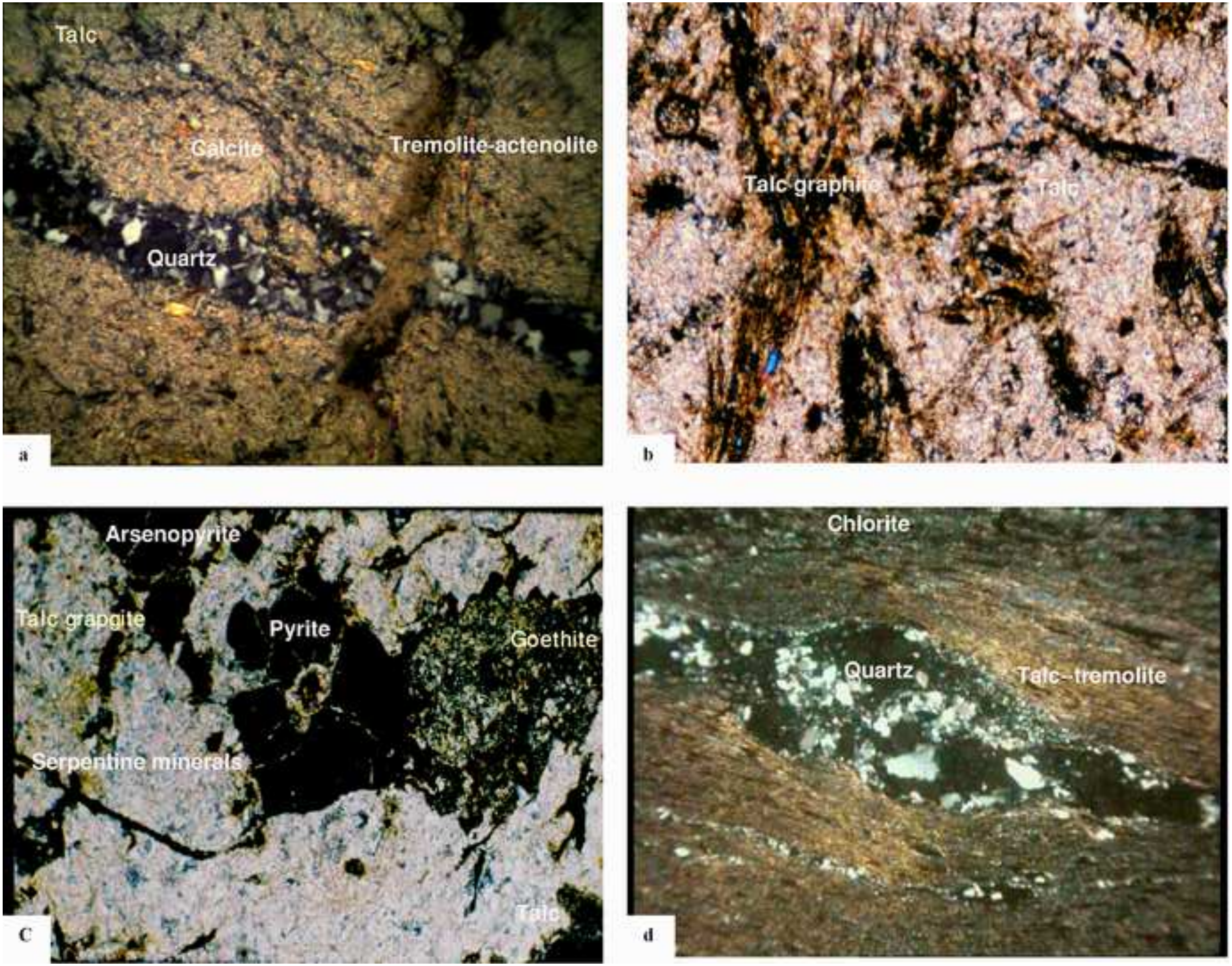

fig.7

Click here to download high resolution image

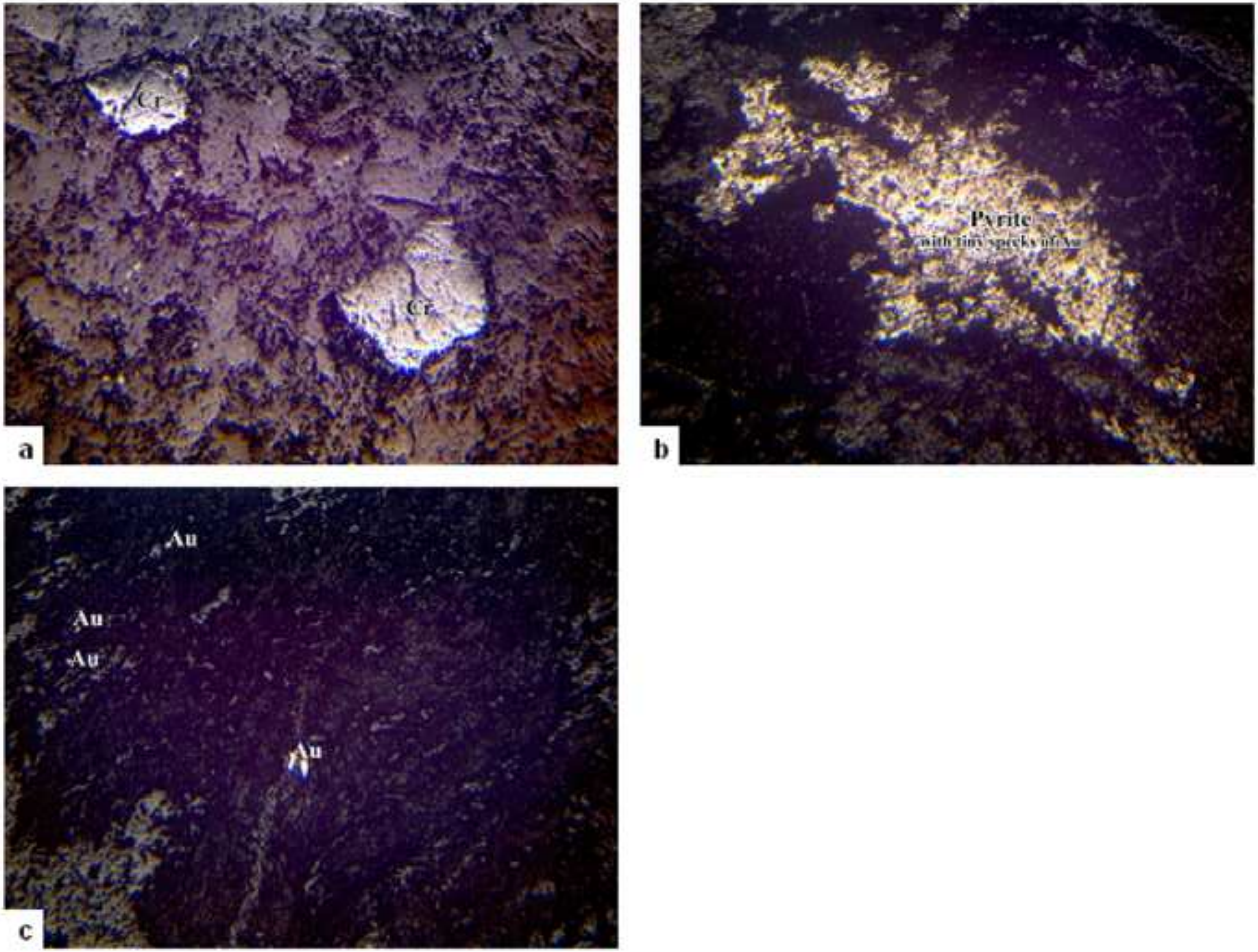

fig.9

Click here to download high resolution image

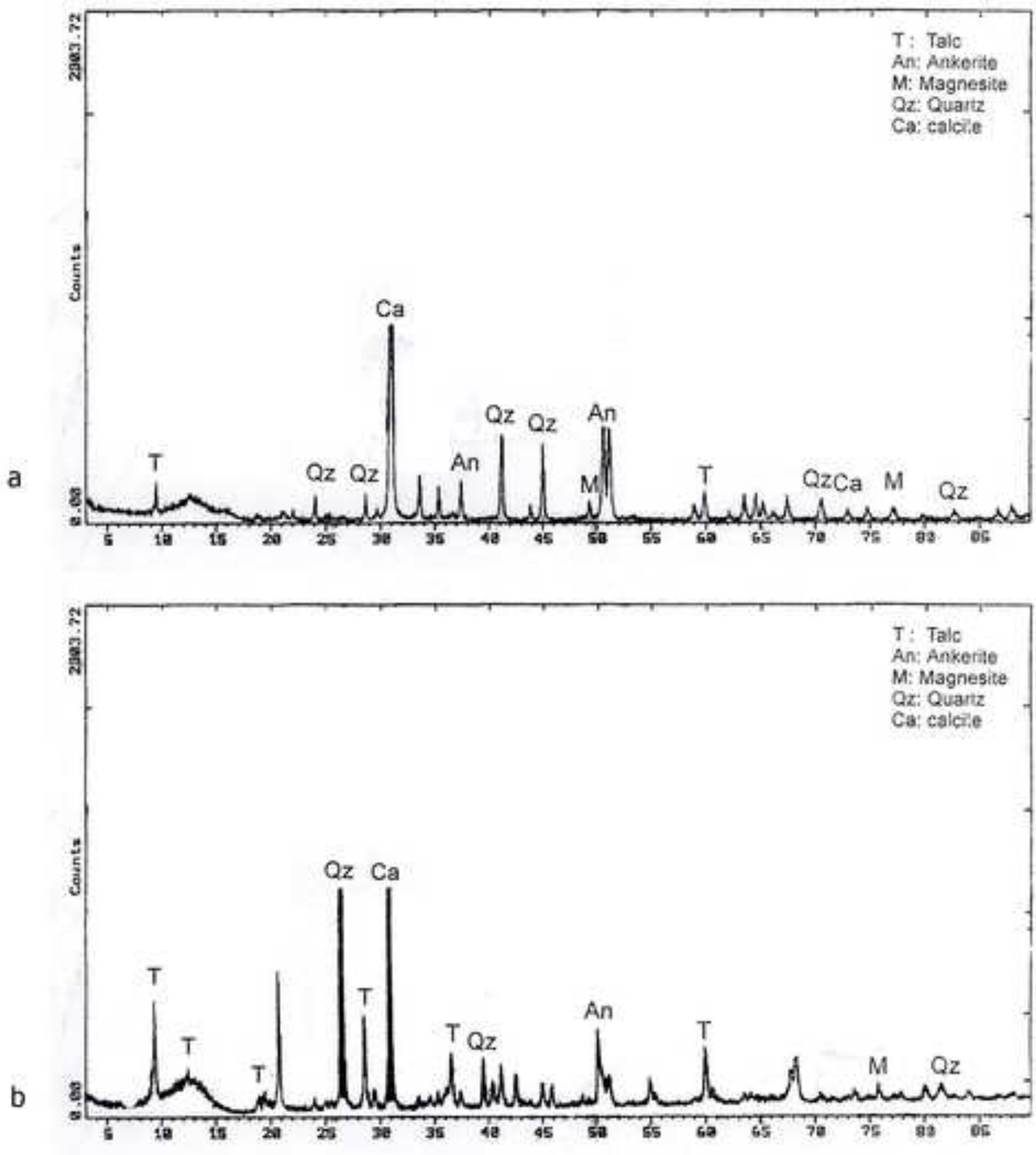

fig.10
Click here to download high resolution image

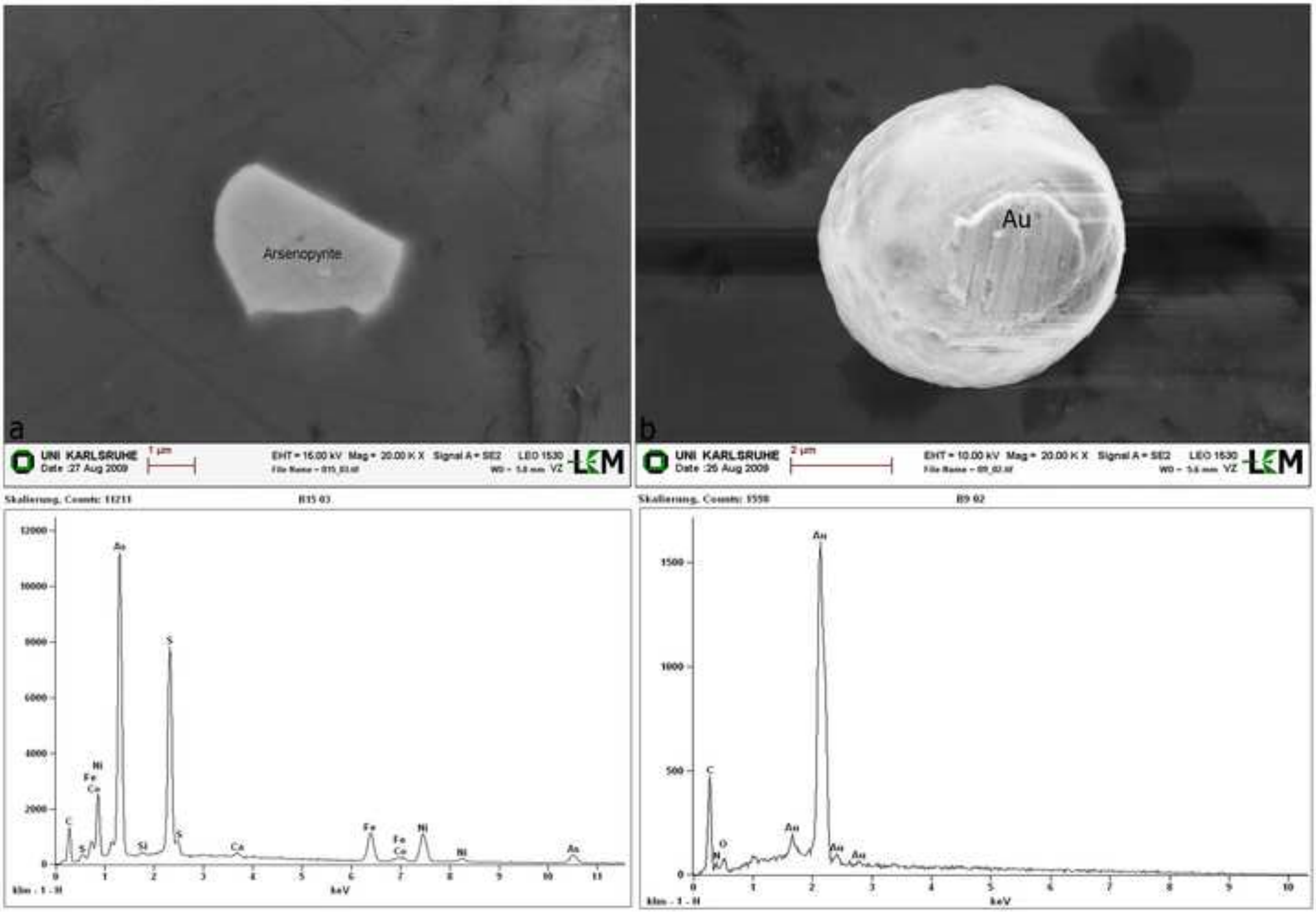

fig.10
Click here to download high resolution image

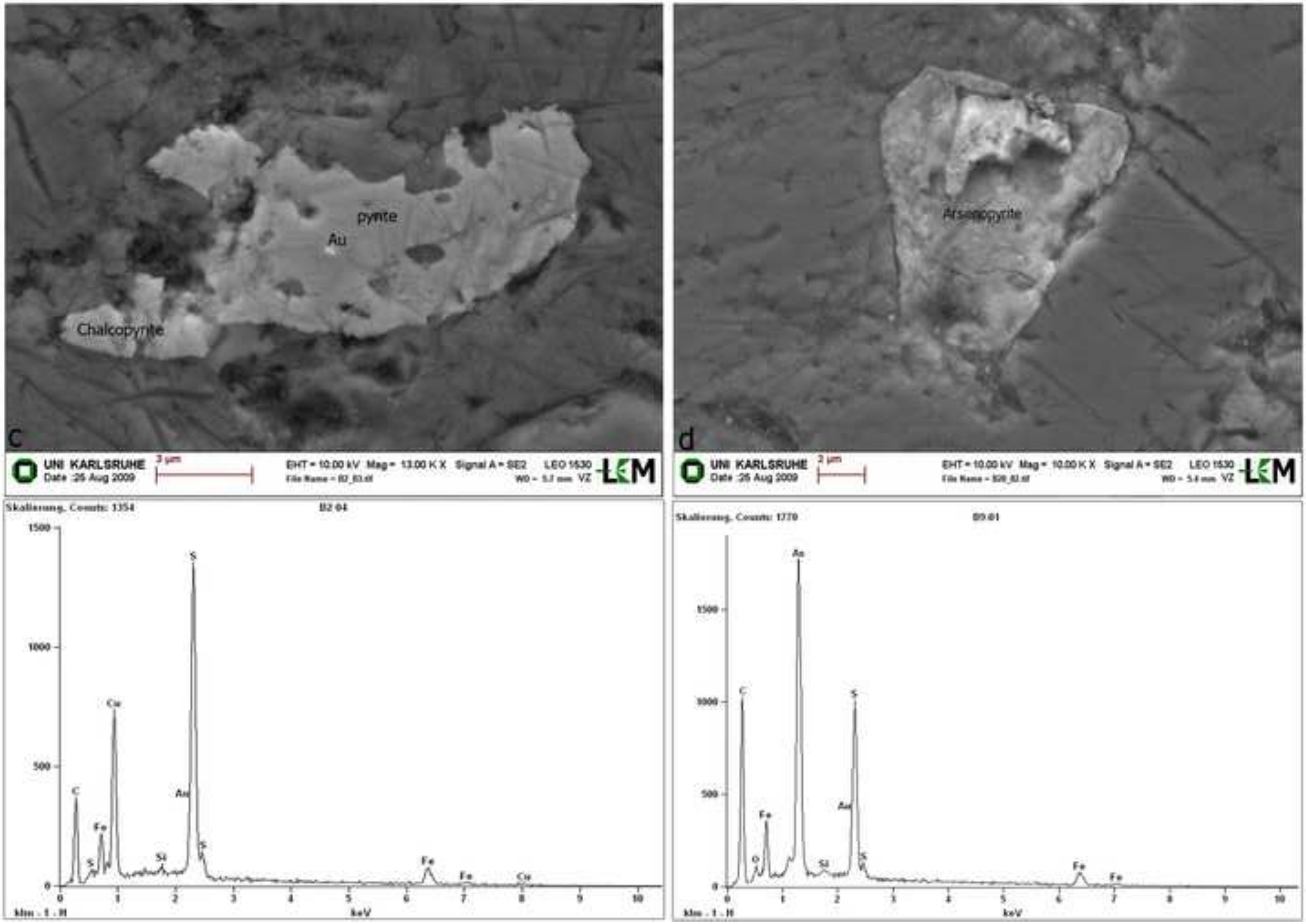

Figure captions

Fig. 1: Location map of the study area.
Fig. 2a: Compiled map interpreted from both ASTER image (unsupervised classification tool) and field observations.
Fig. 2b: Geological map of Barramiya area after Zoheir and Lihman (2011)
Fig. 2c: Vector map converted from the compiled map displaying Nubian sandstone in pale yellow colour.
Fig. 3: Image processing of Barramiya ASTER data. a) False-color composite image of bands (7, 3, 1) in RGB mode (R = 4, G = 6, B = 8) for lihological discrimination. In this color composite the ultramafic rocks appear in dark green colour, the basic metavolcanics in dark brown, the acidic metavolcanics in pale brown, the gabbro-diorite suite in brown, the tonalite in yellowish brown and the Nubian sandstone in the southwestern corner of the mapped area appear in pale greenish brown colour.
b) PC2, PC3 and PC4 image illustrates ENE shear zones control gold mineralization in the Barramiya district.
c) CEM image show the serpentinite locations in the Barramiya district appear as deep brownish red colour. Note, the sinuous reddish zones reflect materials eroded from the serpentinites carried along wadis.
d) SFF of the serpentinites compared with the CEM image of serpentinite locations.
e) RBD of RBD6: (band 4+ band 7)/ (band 6*2) and RBD8 (band7+ band9)/ (band 8*2) recognized the altered Mg-OH and CO3 minerals through the ultramafics appear in light purple colour.
f) Band ratios (4/8, 4/2, 8/9) of the ASTER image detected alteration zone (area1) appear in deep yellowish red colour.
g) Band ratios (4/8, 4/2, 8/9) of the ASTER image detected alteration zone (area2) appear in deep yellowish red colour.

Fig. 4: Some geological features in the Barramiya district. a) NE-SW trending ultramafics (Um) are thrust over the metavolcanics (Mv) at Gabal Barramiya and Gabal Umm Salatit.
b) Development of gold-mineralized listwaenite ridges along thrusts and shear zones.
c) Tonalite intrusion (Ton) penetrating into the metavolcanics (Mv).
d) A well-developed mineral lineation and mylonitic fabrics within the shear zone and tension fractures in the study area.
Fig. 5: Target areas in the Barramiya district. a) View of Barramiya gold mine show trenches, tailings (T) white and waste dumps (D) pale grey.
b) View of alteration zone (area 1).
c) View of alteration zone (area 2).
Fig.6: Petrographic study (Photomicrograph showing); a) Altered minerals of talc calcite and quartz filling fractures in the serpentinites xpl.4x.
b) Fractures in the listwaenites act as paths for mineralized fluids, xpl.4x.
c) Opaque minerals of sulphides and iron oxides in the talc graphite schist, xpl.4x.
d) Augen texture in the dacitic rhyolite rocks along the thrust zones, xpl.4x.
Fig.7: Ore microscopic study (Photomicrograph showing); a) Fractured chromian spinel (Cr) in the talc graphite schist, R.P.L X 320.
b) Pyrite and arsenopyrite with tiny gold inclusion in the talc graphite schist, R.P.L X 320.
c) Fine specks of gold in the listwaenite alterations, R.P.L X 320.
Fig.8, a) Fine specks of gold in the arsenopyrite in the quartz veins, R.P.L X 320.
b) Fine rounded and flakes of gold along fractures in the listwaenites, R.P.L X 320.
c) Tiny inclusion of gold in pyrite in the quartz veins, R.P.L X 320.
d) Fine grained of gold along fractures in the listwaenites, R.P.L X 320.
Fig 9, a) XRD analysis of particular samples from areas 1.

b) XRD analysis of particular samples from areas 2.
Fig.10: Close up view of SEM photomicrographs and their EDAX spot micro-analyses for some rocks (showing); a) Tiny specks of gold in the arsenopyrite in the quartz veins, its microanalysis revealed arsenopyrite, pyrite, nickel and iron.
b) Rounded gold grain in the listwaenite, its microanalysis revealed gold.
c) Tiny specks of gold in the pyrite and chalcopyrite in the quartz veins, its microanalysis revealed pyrite, chalcopyrite and gold.
d) Arsenopyrite ore mineral host tiny specks of gold in the listwaenite, its microanalysis displayed ore minerals of arsenopyrite, pyrite, gold and iron.

Table 1. Wavelength ranges and spatial resolutions of ASTER bands (Abrams, 2000).

Module	VNIR	SWIR	TIR
Spectral bandwidth (µm)	Band 1 0.52–0.60	Band 4 1.650–1.700	Band 10 8.125–8.475
	Band 2 0.63–0.69	Band 5 2.145–2.185	Band 11 8.475–8.825
	Band 3 N 0.78–0.86	Band 6 2.185–2.225	Band 12 8.925–9.275
	Band 3B 0.78–0.86 (backward looking)	Band 7 2.235–2.285	Band 13 10.25–10.95
		Band 8 2.295–2.395	Band 14 10.95–11.65
		Band 9 2.360–2.430	
Spatial resolution (m)	15	30	90

Table 2 Fire assay analysis of five samples from each of the country rocks in the Barramiyya mine

Rock type	Gold content ppm					Average
Graphite schist	9.8	1.76	4.6	2.8	6.3	5.04
Quartz veins	7.4	2.6	1.9	6.8	1.4	4.02
Listwaenite ridges	5.2	3.9	3.2	1.9	4.6	3.76

.

Table 3 Atomic absorption analysis for gold, silver and copper of representative samples from the alteration zone (area 1).

Content	Area 1		
	AU, ppm	Ag, ppm	CU, wt%
Quartz vein			
1	0.6	8	2.1
2	1.6	5	2.9
3	5.2	9	2.5
4	0.8	10	1.6
5	3.7	8	2.7
Average	2.4	8	2.4
Listwaenite			
1	2.6	7	2.8
2	3.9	9	2.9
3	1.2	4	2.9
4	8	10	3.2
5	6.3	10	2.5
Average	4.4	8	2.8

Table 4 Fire assay analysis of five samples from quartz veins and listwaenite alteration of area 1 in the Barramiyya district.

Rock type	Gold content ppm					Average
Quartz veins	2.8	3.4	1.7	5.6	0.9	2.9
Listwaenite ridges	1.2	1.5	1.7	1.1	2.1	1.5

Table 5 Atomic absorption analysis for gold, silver and copper of representative samples from the alteration zone (area 2).

Content	Area 2		
	AU, ppm	Ag, ppm	CU, wt%
Quartz vein			
1	0.8	6	2.2
2	2.6	3	2.1
3	0.7	7	1.8
4	4.8	8	1.7
5	4.4	7	1.8
Average	2.6	6.2	1.9
Listwaenite			
1	1.7	1	1.8
2	1.3	5	2.9
3	6.4	8	3. 4
4	4.7	7	1.1
5	3.3	6	2.7
Average	3.5	5.4	2.4

Table 6 Fire assay analysis of five samples from quartz veins and listwaenite alteration of area 2 in the Barramiyya district.

Rock type	Gold content ppm					Average
Quartz veins	1.9	4.9	3.8	2.5	2.7	3.1
Listwaenite ridges	1.4	1.6	2.3	1.4	1.8	1.7

Highlights

- ASTER images were used to detect two new alteration zones as promising targets for gold exploration in the Barramiya area.
- The field studies verify these alteration zones and their locations in the listwaenite alterations in the northeast (area 1) and southeast (area 2) from the Barramiya gold mine.
- The petrography and ore mineral investigations for representative samples from the alteration zones revealed gold and sulphide bearing gold in the alteration zones samples.
- The geochemical analyses (atomic absorption and fire assay methods) to the same representative samples from the alteration zones support presence of gold in these samples.
- The integration of remote sensing (ASTER images) and field verification supported by geochemical analyses are helpful for gold exploration and be recommended to apply at many arid regions.

fig.8
Click here to download high resolution image